

The benefits of increasing resolution in global and regional climate simulations for European climate extremes

Carley E. Iles¹, Robert Vautard¹, Jane Strachan², Sylvie Joussaume¹, Bernd R. Eggen² and Chris D. Hewitt^{2,3}

¹Laboratoire des Sciences du Climat et de l'Environnement, LSCE/IPSL, CEA-CNRS-UVSQ, Université Paris-Saclay, Gif-sur-Yvette, France

²Met Office Hadley Centre, Exeter, UK

³Centre for Applied Climate Sciences, University of Southern Queensland, Toowoomba, Australia.

Correspondence to: Carley E. Iles (carley.iles@lsce.ipsl.fr)

Abstract. Many climate extremes, including heatwaves and heavy precipitation events, are projected to worsen under climate change, with important impacts for society. Future projections, required for adaptation, are often based on climate model simulations. Given finite resources, trade-offs must be made concerning model resolution, ensemble size and level of model complexity. Here we focus on the resolution component. A given resolution can be achieved over a region using either global climate models (GCMs) or at lower cost using regional climate models (RCMs) that dynamically downscale coarser GCMs. Both approaches to increasing resolution may better capture small-scale processes and features (downscaling effect), but increased GCM resolution may also improve the representation of the large-scale atmospheric circulation (upscaling effect). The size of this upscaling effect is therefore important for deciding modelling strategies. Here we evaluate the benefits of increased model resolution for both global and regional climate models for simulating temperature, precipitation and wind extremes over Europe at resolutions that could currently be realistically used for coordinated sets of climate projections at the pan-European scale. First we examine the benefits of regional downscaling by comparing EURO-CORDEX simulations at 12.5 and 50 km resolution to their coarser CMIP5 driving simulations. Secondly, we compare global scale HadGEM3-A simulations at three resolutions (130, 60 and 25 km). Finally, we separate out resolution dependent differences for HadGEM3-A into downscaling and upscaling components using a circulation analogue technique. Results suggest limited benefits of increased resolution for heatwaves, except in reducing hot biases over mountainous regions. Precipitation extremes are sensitive to resolution, particularly over complex orography, with larger totals and heavier tails of the distribution at higher resolution, particularly in the CORDEX vs CMIP5 analysis. CMIP5 models underestimate precipitation extremes, whilst CORDEX simulations overestimate compared to E-OBS, particularly at 12.5 km, but results are sensitive to the observational dataset used, with the MESAN reanalysis giving higher totals and heavier tails than E-OBS. Wind extremes are somewhat stronger and heavier tailed at higher resolution, except at coastal regions where large coastal grid boxes spread strong ocean winds further over land. The circulation analogue analysis suggests that differences with resolution for the HadGEM3-A GCM are primarily due to downscaling effects.

34 **1 Introduction**

35 Climate extremes, such as heatwaves and heavy precipitation events are projected to worsen under climate change,
36 with important impacts for society (Seneviratne et al., 2012). Such projections are generally based on numerical climate
37 model simulations. However, given finite computational resources, trade-offs between model resolution, ensemble size
38 and the level of model complexity are necessary. For extreme events driven by large-scale processes such as stationary
39 anticyclones, the proper simulation of the amplitude of extremes is limited by dynamics but also by land-atmosphere
40 feedbacks and the many physical processes involved in the surface energy budget. Such extremes are typically heat
41 waves, droughts and cold spells. Many other types of extreme event are by nature small scale, i.e. on the order of a
42 few kilometres to a few hundred kilometres. Such is the case of convective precipitation, flash floods, extratropical
43 wind storms, cyclones and medicanes. These are poorly resolved at the resolution of Global Climate Models (GCMs)
44 in CMIP5 (Coupled Model Intercomparison Project Phase 5; Taylor et al., 2012). Increased resolution in GCMs may
45 improve the representation of small-scale processes and features, including orography and coastlines (downscaling
46 effect), but potentially may also improve the representation of the interaction between small and large scale dynamical
47 processes and ultimately improve the large-scale atmospheric flow (upscaling effect). For instance, a better
48 representation of baroclinic eddies may help to better simulate large Rossby waves such as those inducing long-lived
49 anomalies, due to the inverse energy cascade. This may improve the simulation of the frequency and duration of heat
50 waves and cold spells, and related anomalies such as summer droughts. For precipitation and wind extremes, an
51 improvement with resolution could be expected due to the small-scale processes and features involved, including
52 convection and the influence of topography. However, upscaling effects may also have benefits by improving storm-
53 track location, and duration of wet spells. An alternative approach to increasing the resolution of global-scale models
54 is to use regional climate models (RCMs) driven by coarser GCMs to achieve a given high resolution over a limited
55 area at lower cost. However, this technique only captures downscaling effects, since the RCM inherits the large scale
56 circulation from the driving GCM.

57
58 Current generation GCMs commonly used for climate projections (e.g. CMIP5 models) have a horizontal grid spacing
59 ranging from about 70 to 250 km. Resolution has been increasing further in CMIP6 (Eyring et al. 2016), with some 25
60 km simulations now being run under projects such as PRIMAVERA and HighResMIP (part of CMIP6; Haarsma et
61 al., 2016). For coordinated RCM experiments, such as CORDEX (Coordinated Regional Downscaling Experiment;
62 Giorgi et al., 2009), grid spacing is generally between 10 to 50 km (e.g. Jacob et al., 2014). In order to simulate
63 convective precipitation a grid spacing of <5 km is needed, which is very computationally expensive, but such
64 ensembles of convection permitting RCMs are currently in development (e.g. Coppola et al., 2019; Risanto et al. 2019).
65 An important question is the extent to which increased resolution benefits the simulation of extreme events for both
66 global and regional models for the kind of resolutions that can realistically be run for coordinated pan-continental
67 climate projections. Particularly, whether using global high resolution adds further benefits over regional high
68 resolution due to an improved large scale circulation. We will address these questions focusing on Europe, for which
69 a large number of coordinated RCM simulations at two standard resolutions are available as part of the EURO-
70 CORDEX initiative (Jacob et al., 2014), and whose climate is highly variable and affected by a range of both large and

71 small scale processes, which present challenges for adequate simulation. We focus on extreme precipitation,
72 temperature and wind, to cover a range of phenomena that may be affected by resolution in different ways. Throughout
73 the rest of this manuscript we use the term “resolution” to mean model horizontal grid spacing, whilst recognising that
74 a model’s effective resolution, in terms of the scales it can capture, is always coarser than its grid spacing (Skamarock
75 2004; Klavar et al. 2020).

76
77 The benefits of increased resolution for European precipitation extremes are well documented, whilst the effects on
78 heatwaves, cold spells and wind extremes are less well known. In GCMs, global precipitation tends to increase with
79 resolution, and for grid point GCMs (as opposed to spectral GCMs) the fraction of land precipitation and moisture
80 fluxes from land to ocean increases, largely due to better resolved orography (Vannière et al., 2019; Terai et al., 2018;
81 Demory et al., 2014). Precipitation extremes tend to get heavier and in some studies agree better with observational
82 estimates with increased resolution (Wehner et al., 2010, O’Brien et al., 2016; Kopparla et al., 2013; Shields et al.,
83 2016; Vannière et al., 2019; Demory et al. 2020; Strandberg and Lind 2020), unless the parameterisation schemes are
84 not suited to the resolution (e.g. Wehner et al., 2014 and possibly Bador et al. 2020, who found worse performance in
85 higher resolution versions of multiple GCMs whose parameterisations were not retuned at higher resolution,
86 particularly in the tropics). In Europe, Schiemann et al. (2018) find that both mean and extreme precipitation are
87 simulated better with increased resolution in HadGEM3A, mostly originating from better resolved orography. In
88 contrast, Van Haren et al. (2015a) find that improvements in Northern and Central European mean and extreme winter
89 precipitation with resolution are mostly associated with improved storm tracks in EC-Earth. For RCMs, extreme
90 precipitation is improved with resolution when compared to high resolution observations, particularly over complex
91 orography, including frequency-intensity distributions and spatial patterns, (e.g. Torma et al., 2015; Prein et al., 2016;
92 Ruti et al., 2016; Fantini et al. 2018). However, benefits are smaller for regional and seasonal mean precipitation.
93 Convection permitting models (<4km grid spacing) are particularly beneficial in simulating summer extreme and sub-
94 daily precipitation, including the diurnal cycle of convection, but can overdo extreme precipitation (e.g. Prein et al.,
95 2015; Kendon et al., 2012; 2014).

96
97 For heatwaves, increasing horizontal resolution does not lead to obvious benefits in RCM simulations (see e.g. Vautard
98 et al., 2013 for EURO-CORDEX), except improved spatial detail (Gutjahr et al., 2016). However, increased resolution
99 may have more impact in global models since the large scale circulation that contributes to heatwave formation may
100 be affected. This remains a largely unstudied question, with the exception of a few studies such as Cattiaux et al. (2013)
101 who find that increasing resolution in the IPSL GCM leads to a reduction in the cold bias of both cold and warm
102 extremes in Europe, along with improved statistics, such as duration and frequencies and improved weather regimes.

103
104 For wind extremes, stronger winds and better spatial detail with resolution have been found for regional models (e.g.
105 Pryor et al., 2012; Kunz et al., 2010). Donat et al. (2010) found that observed storm loss estimates for Germany could
106 be reconstructed more accurately through dynamical downscaling compared to using the coarser resolution driving
107 ERA-40 data directly. Ruti et al., (2016) found improvements in Mediterranean cyclogenesis in coupled Med-
108 CORDEX RCMs relative to the ERA-interim driving data, whilst extreme winds over the Mediterranean generally

109 improve (i.e. are stronger) with higher resolution RCMs (e.g. Ruti et al. 2016; Hermann et al. 2011). Most GCM studies
110 focus on the simulation of extratropical cyclones rather than wind directly. Such studies find an improvement in the
111 representation of various aspects of Northern Hemisphere extratropical cyclones with increased resolution, including
112 frequency, intensity and the position of the storm tracks (Colle et al., 2013; Jung et al., 2006; 2012), even in the higher
113 resolution CMIP5 models ($\sim < 130$ km; Zappa et al., 2013). Vries et al., (2019) found that the resolution of Atlantic
114 Gulf-Stream SST fronts affects winter extratropical cyclone strength. Gao et al (2020) found that explosively
115 intensifying “bomb” extratropical cyclones are more frequent and associated with stronger winds in higher resolution
116 GCMs. Whether the aforementioned improvements translate into an improvement in wind extremes remains to be
117 assessed.

118
119 Persistence of weather regimes, such as blocking or the phase of the North Atlantic Oscillation, can be important
120 drivers for extreme events in Europe. Using the ECMWF IFS model, Dawson et al., (2012; 2015) find that such weather
121 regimes cannot be simulated realistically at typical CMIP5 resolution (~ 125 km grid spacing), but are improved at 40
122 km, and well-simulated at 16 km. Cattiaux et al., (2013) find improvements at more modest resolutions in the IPSL
123 model. However, multi model GCM analyses by Strommen et al. (2019) and Fabiano et al. (2020) suggest that only
124 some aspects of weather regimes are systematically improved with resolution, and that these aspects are not consistent
125 between atmosphere only or coupled GCMs. Blocking frequency tends to be underestimated by CMIP5-resolution
126 climate models (Anstey et al., 2013). This tends to be somewhat improved with resolution, particularly over the North
127 Atlantic (Jung et al., 2012, Anstey et al., 2013; Matsueda et al., 2009, Berckmans et al., 2013, Davini et al., 2017a;
128 2017b; 2020; Strommen et al. 2019; Schiemann et al. 2020), although results tend to be somewhat sensitive to season
129 and model considered (Schiemann et al., 2017) and compensating errors may be involved (Davini et al., 2017a for EC-
130 EARTH). O’Reilly et al. (2016) find that having a well-resolved Gulf stream SST front is also important for European
131 winter blocking and associated cold spells. An important question is whether these improvements in the large scale
132 circulation translate into an improvement in the simulation of European climate extremes.

133
134 Here we examine the benefits of increased resolution for global and regional models for the simulation of European
135 temperature, precipitation and wind extremes. We further break down any resolution related differences for a global
136 model into upscaling and downscaling components. This will shed light on whether potential improvements in the
137 large scale circulation suggested in the literature translate into an improved representation of climate extremes. This is
138 an important consideration in choosing how to distribute finite resources between global and regional models. We
139 focus on the kind of models widely used to provide climate projections at a European scale, applying a consistent
140 approach across model types. Firstly, the benefits of regional dynamical downscaling are explored by comparing
141 EURO-CORDEX simulations at 50 and 12.5 km resolutions to their coarser driving CMIP5 GCMs. Secondly, the
142 benefits of increased resolution for a global model are examined using HadGEM3-A at 130, 60 and 25 km resolution.
143 Finally, the roles of upscaling versus downscaling will be examined using a circulation analogue technique applied to
144 HadGEM3-A.

145 **2 Observational and model data**

146 **2.1 Observational data**

147 Model simulations are evaluated using observational and reanalysis datasets. For daily precipitation and daily
148 maximum temperature, we use the gridded station based dataset E-OBS v15 on a 0.5° latitude-longitude grid (Haylock
149 et al. 2008). This covers the European domain from 1950 to present. Gridded datasets tend to reduce the magnitude of
150 extremes compared to station data through smoothing effects, but are more comparable to the grid box averages from
151 GCMs (Haylock et al. 2008). E-OBS has a somewhat non-uniform underlying station density, with relatively high
152 densities in Germany, Sweden and Slovenia, and low densities in other countries (e.g. Spain, France, Austria). It tends
153 to underestimate precipitation extremes relative to higher density regional datasets, especially where it has poor
154 coverage, due to missed extremes which are local in scale (Prein and Gobiet 2017; Herrera et al. 2019). However, such
155 high resolution datasets are not available at a pan-European scale. As a compromise, results are repeated for
156 precipitation extremes using the 5.5 km resolution MESAN reanalysis (Landelius et al. 2016), which adjusts a
157 downscaled first guess from the 22km resolution HIRLAM reanalysis (Dahlgren et al. 2016) with a network of station-
158 based precipitation observations. For much of Europe these are the same as those used for E-OBS, but with the addition
159 of Swedish Meteorological and Hydrological Institute (SMHI) stations over Sweden, and a high density of Meteo-
160 France stations over France (Landelius et al. 2016). MESAN provides daily precipitation data for the more limited
161 period 1989-2010. Prein and Gobiet (2017) find that it gives heavier extremes than E-OBS in some regions (France,
162 Spain, the Carpathians), but generally not as high as the high resolution regional datasets (except in France). Neither
163 dataset is corrected for gauge undercatch, which tends to be around 3-20% for rain, and up to 40% for snow, or even
164 80% for non-shielded gauges (Førland and Institutt 1996; Goodison et al. 1997).

165
166 Wind extremes tend to happen on sub-daily time scales, necessitating the use of sub-daily data to avoid missing as
167 many events (although events, or their peak magnitude, will still be missed). We use 10 m wind speed from three
168 reanalysis datasets. These are the EURO4M DYNAD (Landelius et al. 2016), UERRA MESCAN-SURFEX (Bazile et
169 al. 2017) and ERA5 (Hersbach et al. 2019) reanalyses. The former is available at 6 hourly intervals on a 5.5km rotated
170 grid over Europe for the period 1979-2013 and is computed through dynamical adaptation of a downscaled version of
171 the 22km resolution HIRLAM reanalysis to 5.5 km resolution orography using DYNAD (a simplified version of
172 HIRLAM). MESCAN is also available at the same spatial and temporal resolution over Europe from 1961 onwards,
173 but is computed through dynamical downscaling of the 11 km UERRA-HARMONIE reanalysis. Both HIRLAM and
174 UERRA-HARMONIE are forced by the ERA interim global reanalysis (ERA40 before 1979 for the latter). Finally,
175 ERA5 is available globally at 0.25° and at hourly resolution from 1979 onwards. We sub-sample ERA5 to 6 hourly
176 data by taking every sixth value in order to be consistent with the other reanalyses.

177

178 **2.2 Climate model data**

179 **2.2.1 EURO-CORDEX and CMIP5**

180 In order to examine the effect of dynamical downscaling for climate extremes, we make use of the EURO-CORDEX
181 (Jacob et al. 2014) RCM simulations for the historical period over the European domain which are driven by lower
182 resolution global scale coupled CMIP5 GCMs. The GCMs are forced by observed records of anthropogenic and natural
183 forcings, such as greenhouse gases, anthropogenic aerosols, land use changes, solar variability and volcanic aerosols
184 to allow comparability to historical records. For the most part the RCMs inherit the effects of these forcing agents from
185 the GCMs, with the exception of greenhouse gases, which are prescribed. A comparison of the RCM simulations with
186 their driving CMIP5 simulations allows us to identify any value added by regional high resolution. The EURO-
187 CORDEX simulations are available at 0.11° and 0.44° (12.5 km and 50 km respectively), allowing an assessment of
188 the difference that increased regional resolution brings. Simulations are performed with the same model versions and
189 parameterisations for both resolutions, except for REMO where rain advection is used at 0.11° but not 0.44° (Kotlarski
190 et al. 2014). By examining the subset of GCM-RCM combinations that are common to both CORDEX resolutions
191 along with their driving GCMs we can isolate the effects of changing resolution. Hereafter, this subset is referred to as
192 the “common subset”. We also examine how representative the results for this common subset are by recalculating
193 them using all available CMIP5 and CORDEX simulations, using one member per model.

194
195 Daily precipitation (pr), daily maximum temperature (tasmax), and 3 hourly wind (sfcWind) were taken from both
196 CORDEX and CMIP5. For wind, every other time step was taken in order to obtain 6 hourly data to be consistent with
197 the reanalysis data. The simulations used are shown in Table S1. These consist of 23 and 19 simulations for
198 precipitation for the 0.44° and 0.11° CORDEX simulations respectively, with 15 in the common subset; 22 and 18
199 respectively for temperature, with 14 in the common subset. For wind, data were very limited for CORDEX at 0.44°
200 and there was no overlap of models with those used for the 0.11° simulations. Therefore, the wind analysis in the main
201 manuscript is based only on CORDEX 0.11° and CMIP5. There were 31 simulations for wind for CORDEX 0.11°,
202 with 15 in the common subset. CORDEX 0.11° and 0.44° were compared instead using the variable sfcWindmax (daily
203 maximum wind) which was available for 9 models at both resolutions (see Figure S8). There seemed to be
204 inconsistencies in the way sfcWindmax was calculated between CMIP5 models (mostly yielding stronger annual
205 maximum winds compared to using 3 hourly data to varying extents, but sometimes weaker), which precluded basing
206 the full analysis on this variable. When calculating ensemble medians for the common subset of simulations, we
207 repeated GCM members that drive more than one RCM. The number of CMIP5 simulations used for the extended
208 ensemble was 44 for precipitation, 42 for temperature and 25 for wind.

209

210 **2.2.2 UPSCALE simulations**

211 In order to examine the benefits or otherwise of differences in resolution for a global model, we make use of simulations
212 undertaken as part of the UPSCALE project (UK on PRACE: weather-resolving Simulations of Climate for globAL
213 Environmental risk; Mizielinski et al. 2014). This consists of the atmosphere only version of the Hadley Centre Global

214 Environment Model 3 (HadGEM3-A) run at three different resolutions: N96 (130 km), N216 (60 km) and N512 (25
215 km), all with 85 vertical levels for the period 1985-2011, with 5, 3 and 5 ensemble members respectively (or 3, 3 and
216 5 for wind data). The simulations are forced by observed records of greenhouse gases, aerosols, ozone, solar variability
217 and volcanic forcings following the AMIP-II procedure (Taylor et al. 2000), but using the higher resolution OSTIA
218 analysis (Operational Sea Surface Temperature and Sea Ice Analysis) for sea surface temperatures (SSTs) and sea ice
219 (Donlon et al. 2012). Very few parameters differ between the resolutions, enhancing the comparability of the three
220 ensembles. We use daily precipitation data, daily maximum temperatures and 3-hourly wind (subsampled to 6-hourly).

221 **2.3 Regridding**

222 In order to compare models of different resolutions with each other and with the observational datasets it was necessary
223 to regrid variables to a common grid. Using a high resolution grid for evaluation would preserve the finer spatial detail
224 and localised extremes for high resolution simulations, but is sometimes considered unfair for coarse resolution models
225 which cannot be expected to simulate the same intensities of extremes even for a perfect simulation due to spatial
226 smoothing effects. If processes are captured better at higher resolution, improvements should still be visible when
227 regridded to coarser resolution (Prien et al. 2016; Fantini et al. 2018). However, the finer spatial detail is an inherent
228 advantage of high resolution and smoothing this out will result in partial information loss. We use the 0.5° regular
229 longitude-latitude grid of E-OBS since it is in-between the resolution of the CORDEX models and CMIP5, and is
230 computationally feasible. Some of the benefits of higher resolution may be lost by doing this, putting our results on
231 the conservative side. Nevertheless, sensitivity tests showed that results for MESAN did not change perceptibly by
232 using a 0.5° grid compared to a 0.1° grid. We regrid the daily data, before the calculation of annual extreme indices.

233
234 The sensitivity of the results to the regridding technique was investigated for a number of models of different
235 resolutions and compared to results based on using the original grids (Figure S1). For the coarser resolution models
236 (e.g. HadCM3) results for precipitation extremes were particularly sensitive to the regridding technique, with much
237 weaker extremes for some techniques e.g. distance-weighted average remapping and bilinear interpolation, with
238 unrealistic artefacts in the spatial patterns for many methods. For high resolution models, the regridding technique did
239 not make much difference to the results, although conservative remapping tended to dampen extreme precipitation,
240 particularly for CORDEX 0.11. Overall the nearest neighbour method was chosen for precipitation for everything
241 except CORDEX 0.11 and MESAN since it gave results very close to using the original grid for all model resolutions,
242 preserving the amplitude of extremes, and also having minimal artefacts when plotting spatial patterns of precipitation
243 extremes. For going from high to lower resolution (e.g. 0.11° to 0.5°) nearest neighbour is less appropriate since
244 information from only a subset of grid cells is incorporated. Therefore, bicubic remapping was used for CORDEX 0.11
245 and MESAN, which also replicated results using the original grid very well (Figure S1). Wind and temperature results
246 were also somewhat sensitive to regridding technique, particularly for the coarser models. The above choices also
247 seemed appropriate for these variables (nearest neighbour in most cases, but bicubic for CORDEX 0.11, MESCAN,
248 ERA5 and DYNAD), both in terms of replicating return period results using the original grid, and retaining the blocky
249 nature of the low resolution simulations in the spatial patterns.

250 **3 Methods**

251 **3.1 Extremes Indices**

252 In order to examine extremes, we adopt indices based on the ETCCDI indices (Zhang et al. 2011). For precipitation
253 these are the annual maximum daily precipitation (Rx1day) and the annual maximum consecutive 5-day total
254 (Rx5day). For temperature we use the annual maximum daily maximum temperature (TXx) and the annual maximum
255 consecutive 5-day mean of daily maximum temperature (TXx5day). Rx1day and TXx5day are presented in the figures,
256 whilst the other indices are commented on in the text. For wind we use the annual maximum of daily maximum wind,
257 which we refer to as (WindXx). This is based on 6-hourly data. These are therefore much rarer extremes than those
258 based e.g. on the 95th or even 99th percentile which would happen on average 1 in 20 days and 1 in 100 days
259 respectively. One drawback is that this makes robust statistics more challenging.

260
261 In order to examine how well the climate models simulate extremes and the differences between different resolutions,
262 we first examine the spatial patterns of the climatological mean values of the indices and their biases with respect to
263 observational datasets. We then examine return period plots (see definitions below) for a number of regions for each
264 index, which highlights any differences in the shape of the tails of the distribution of the extremes. The regions used
265 are based on the PRUDENCE regions (Christenson and Christenson 2007) and the IPCC SREX regions (Seneviratne
266 et al. 2012) and are shown in Figure S2 and Table S2. A subset of representative regions are presented here, with some
267 comments about the others.

268 **3.2 Return periods**

269 In order to calculate regional return periods and return values we first sort the data into ascending order for each grid
270 cell. The return periods are calculated as N/k where N is the number of years of data, and k is the rank, with $k=1$ for
271 the largest value. Return periods are therefore the inverse of the probability of an event exceeding a given value (called
272 the “return value”). This is an empirical approach and has the limitation that return periods cannot exceed the number
273 of years of data used (e.g. 36 years). This is still the case even if an extremely unusual event occurs. Fitting a GEV
274 would allow estimates for higher return periods, but this would still be an extrapolation. The area weighted regional
275 average is made, for given return periods, over the associated return values. To avoid complications from missing data,
276 grid cells in E-OBS with more than 5 days of missing data in any year during the period examined were masked for
277 the whole period. Having one or more years missing would complicate the calculation of regional mean return periods
278 and values. Models and observational datasets are masked to have the same spatial coverage, which is land only. A
279 common time period across the models being examined and the observations they are being compared to is chosen to
280 allow comparability. For the CMIP5 and CORDEX analysis 1970-2005 is used for temperature and precipitation and
281 1979-2005 for wind. For the UPSCALE runs we use 1985-2011 for temperature, and 1989-2010 for precipitation to
282 allow comparisons with MESAN (1986-2011 is used for the analogue analysis, see below) and 1986-2011 for wind.

283
284 In order to allow the shapes of the return period curves to be compared more easily between different types of models
285 (i.e. CMIP5 and CORDEX at both resolutions), we first adjust each model to have the same climatological mean value

286 of the extreme index in question. This effectively shifts the curves up or down, but does not change their shape, which
287 is the focus of these figures. Without such a shift, curves are too spread out to be able to discern differences in shape.
288 Therefore we cannot comment on mean biases of the extremes indices based on the return plots, but these biases are
289 already shown and discussed based on map figures (see section 3.1). We implement this adjustment by subtracting the
290 difference between the model climatology of the index in question and the climatology of the reference observational
291 dataset for each model at a grid cell level. We use E-OBS as the reference for temperature and precipitation, and
292 MESCAN for wind. The additional observational datasets shown in the return period plots are also adjusted in the
293 same way. For the UPSCALE simulations, results can also be examined without the need to shift the curves to a
294 common mean value because the same version of the same model is used for a given resolution, meaning that curves
295 for individual simulations tend to cluster together instead of having large mean differences. In this way, differences in
296 biases with resolution are also seen in the return period plots. Nevertheless, we also present UPSCALE results with
297 the adjustment in Figure S10 for comparison.

298
299 Confidence intervals for the observational datasets are calculated using a bootstrapping method. If, for example, the
300 analysis period was 1970-2005 (i.e. 36 years), 1000 random samples of 36 years from this period are chosen from the
301 same dataset, allowing the same year to be chosen more than once per iteration. For each random sample, the chosen
302 values are sorted for each grid cell and a regional average is calculated as above, effectively yielding 1000 return period
303 curves per region. The 5th and 95th percentile of these values are then calculated to give the confidence intervals.

304

305 **4 Results**

306 **4.1 The benefits of regional high resolution: EURO-CORDEX versus CMIP5**

307 **4.1.1 Temperature extremes**

308 Figure 1 shows the spatial patterns of the climatological mean of TXx5day for the period 1970-2005 for E-OBS, and
309 the multi-model medians (MMM) of CMIP5, and CORDEX at both resolutions, along with their biases with respect
310 to E-OBS. The same general pattern can be seen in both E-OBS and the models, with hotter extremes in the south and
311 cooler extremes in the north and over the mountains. At higher resolution the colder warm extremes over the Alps and
312 Carpathians become more distinct. For the “common subset” the pattern of biases relative to E-OBS is similar for both
313 CMIP5 and CORDEX with cold biases in the North and West and hot biases in the South-East. However, the hot biases
314 over the mountains reduce with higher resolution since the model topography is higher. The cold bias over Scandinavia
315 is also larger in CORDEX than in CMIP5. Biases for CORDEX using the whole ensemble are similar to those for the
316 common subset. For CMIP5 the hot biases over the south-east, and over mountain ranges are stronger when using all
317 simulations compared to the subset. Findings for TXx are similar, but hotter (not shown).

318

319 To give an idea of the level of consistency of results between models, results for individual models are shown in Figure
320 S3. Although the CMIP5 models agree on the general spatial pattern of temperature extremes, their absolute

321 magnitudes vary considerably, although all are too hot over the Alps. There are also substantial differences between
322 results from different RCMs, including those driven by the same GCM, although the driving GCM does seem to affect
323 the overall magnitude of the temperature extremes. Biases of individual RCMs do not appear systematically smaller
324 than that of their driving GCM. Patterns are very similar for the same GCM-RCM chains at the both 12.5 and 50 km
325 resolutions. Results for different ensemble members of the same GCM or GCM-RCM chain are very consistent,
326 suggesting that the differences between models are not due to internal variability.

327
328 In order to assess any effect of resolution on the shape of the tails of the statistical distribution of temperature extremes,
329 Figure 2 (left column) shows return period against magnitude for TXx5day for CMIP5, CORDEX at both resolutions
330 and E-OBS (see Methods). Results are shown for Northern, Central and Southern Europe, and are representative of
331 results for the smaller PRUDENCE regions that fall within their boundaries. There is no obvious difference in the
332 shape of the tails between CMIP5 and CORDEX. Agreement with E-OBS is good for the multi model median, although
333 many individual ensemble members lie outside the range of the observational uncertainty.

334
335 In summary, shapes of return period curves for temperature extremes appear to be insensitive to dynamical
336 downscaling based on comparing CMIP5 to CORDEX at 0.11° and 0.44°, but biases are affected, for instance over
337 mountains where hot biases decrease with resolution.

338 **4.1.2 Precipitation extremes**

339 Now we consider precipitation extremes for CMIP5 compared to CORDEX. Figure 3 shows the climatological mean
340 of Rx1day for E-OBS and the MMMs of CMIP5 and CORDEX at both resolutions, and their differences with respect
341 to E-OBS. The heaviest annual maximum precipitation totals in E-OBS occur over the Alps and the western side of
342 coastal mountain ranges, including western Norway and north-eastern Spain. A similar spatial pattern of precipitation
343 distribution can be seen in the models, although totals are lower in CMIP5, and higher in CORDEX. CMIP5 is drier
344 than E-OBS over most of Europe, particularly over the areas of maximum observed precipitation (i.e. over or near
345 mountains), whilst CORDEX is generally wetter than observed, particularly in these same locations, and at higher
346 resolution. Results using the entire ensembles are very similar to using the common subset of simulations. Previous
347 studies suggest that E-OBS underestimates precipitation extremes since it is not corrected for gauge undercatch and
348 has a relatively low underlying station density (e.g. Prein and Gobiet 2017). Therefore, we also repeat the analysis
349 using the MESAN reanalysis as the reference (Figure S4) for the shorter period 1989-2005. MESAN uses a particularly
350 high density of stations in France (see Data section). The climatology of Rx1day is wetter in MESAN than in E-OBS
351 over most of Europe, most noticeably over the Alps and surrounding areas. This leads to the dry bias in CMIP5
352 appearing bigger, and the wet bias in CORDEX decreasing, although it is still present in the 0.11° simulations. Using
353 regional-scale very high resolution datasets could improve agreement with the 0.11° simulations, since they tend to
354 give heavier precipitation extremes (Prein and Gobiet 2017). Gauge undercatch will also contribute to the difference,
355 particularly for precipitation extremes associated with strong winds and in snow dominated regions

356

357 Figure S5 shows results for individual models. Again, whilst models agree on the general pattern of precipitation
358 extremes – i.e. wettest over mountains, there are considerable inter-model differences concerning the magnitude,
359 particularly over complex orography. A number of CMIP5 models have too light extremes everywhere, but all
360 underestimate precipitation extremes over mountainous regions to a greater or lesser extent. RCMs systematically
361 simulate heavier precipitation extremes compared to their driving GCMs, particularly over mountains, and these
362 extremes tend to become heavier when moving from 0.44° to 0.11° in most cases. Many of the RCMs have heavier
363 precipitation extremes than seen in E-OBS over much of Europe at 0.44°, although this difference may disappear if
364 compared to MESAN. This difference gets bigger at higher resolution and is largest over mountainous regions. The
365 spatial patterns seem to be very RCM-dependent, with limited influence of biases in the driving GCM. Again results
366 are very consistent between ensemble members of the same models.

367
368 Figure 2 (middle column) shows return period curves for Rx1day for Northern, Central and Southern Europe. There is
369 a clear separation in the tails of the distribution according to resolution, with CMIP5 having the lightest tails, CORDEX
370 0.44 in the middle, and CORDEX 0.11 with the heaviest tails across all regions (including the smaller PRUDENCE
371 regions – not shown). Results using the common subset of models or the full ensembles are similar to each other. E-
372 OBS tends to lie between CMIP5 and CORDEX 0.44 for southern Europe, and closer to CORDEX 0.44 in central and
373 northern Europe. Using MESAN gives slightly heavier tails in all three regions, particularly in southern Europe (Figure
374 S6) and France where station density is highest (not shown), causing the best agreement to occur with CORDEX 0.44
375 everywhere. Results for Rx5day are similar, but with marginally less separation between the resolutions, whilst over
376 Northern and Central Europe the best agreement with E-OBS happens at a slightly higher resolution than for Rx1day
377 – i.e. either with CORDEX 0.44 or the lower end of the range of CORDEX 0.11 (not shown).

378
379 In summary, precipitation extremes are wetter and heavier tailed with higher resolution, especially over mountainous
380 regions. CMIP5 has a dry bias, particularly over mountains, whilst CORDEX tends to be too wet relative to E-OBS,
381 particularly at 0.11°, but results are sensitive to observational dataset used, with wet biases for CORDEX reducing
382 when compared to the higher resolution MESAN dataset.

383 4.1.3 Wind Extremes

384 Finally, we examine annual maximum wind (WindXx). Figure 4 shows the multi model medians of climatological
385 mean annual maximum wind for CMIP5 and CORDEX at 0.11° compared to three reanalysis datasets. Data for
386 CORDEX 0.44° were very limited and did not overlap with the models used at 0.11°- therefore those results are not
387 shown. The MESCAN and DYNAD reanalyses show strong extreme winds over the UK, the Norwegian mountains
388 and the NW coastline of France through to Denmark. Relatively strong winds are also seen over the Spanish plateau,
389 and a belt of strong winds running zonally across central Europe between somewhat slower winds to the North and
390 South. The datasets differ in the magnitude of the winds, with DYNAD having more contrast between areas of low
391 and high wind. MESCAN should be the more accurate of the two (Tomas Landelius, personal communication). ERA5
392 has notably slower winds, particularly over mountainous regions, but a similar overall zonal tripole pattern can be

393 seen. Niermann et al (2017) found that MESCAN underestimates extreme winds compared to station data over
394 Germany. ERA5 must therefore underestimate even more. Concerning mean winds, Jourdiere (2020) find that ERA5
395 underestimates wind speed compared to French stations, particularly over mountains.

396
397 The CMIP5 driving model median shows a similar overall pattern of WindXx as the reanalyses, particularly ERA5,
398 with a pattern of weaker winds in the north and south, and a belt of stronger winds in the middle. However, CMIP5
399 does not tend to have stronger winds over mountains like in DYNAD and MESCAN. Using the whole CMIP5 ensemble
400 gives similar results. The CORDEX multi model medians show generally higher wind speeds than CMIP5, and
401 captures the high wind speeds along western coastlines and over some mountainous terrain. Results for the common
402 subset of simulations are similar to those obtained from the complete CORDEX ensembles, except that the latter shows
403 slow wind speeds over the Alps instead of high. This latter feature is very RCM-dependent, and indeed the overall
404 pattern and magnitude of the extreme winds almost entirely reflects the choice of RCM with very little influence of
405 GCM (Figure S7). For some RCMs the zonal tripole pattern is the clearest feature (ALADIN, COSMOcrCLIM), whilst
406 for others it is the high winds over mountains and coastlines (RCA, HIRHAM5). The driving GCMs differ considerably
407 in terms of the magnitude of extreme winds, but have a similar overall pattern to each other (Figure S7). Ensemble
408 members of the same model give very similar results for both CORDEX and CMIP5. Multi-model median biases are
409 dependent on the reanalysis used for reference, with CORDEX 0.11 being close to DYNAD, and CMIP5 being closest
410 to ERA5. In order to compare the two resolutions of CORDEX, results based on sfcWindmax instead of 3 hourly wind
411 are presented in Figure S8 (see methods). Winds are either similar between the two resolutions (e.g. RCA and WRF),
412 or stronger at higher resolution (RACMO, HIRHAM5). Again the overall pattern is very RCM-dependent.

413
414 Figure 2 (right column) shows return period plots for WindXx for CMIP5 and CORDEX at 0.11°. The British Isles
415 are shown instead of Northern Europe, since they are particularly affected by wind extremes, and for comparison with
416 the results for the UPSCALE simulations, where this region shows distinctive results. The distribution of annual
417 maximum sfcWindmax has somewhat heavier tails in CORDEX 0.11 compared to CMIP5, regardless of the subset of
418 models used in calculating the multi-model median in all regions examined. CORDEX 0.11 tends to be closest to
419 DYNAD and MESCAN, whilst CMIP5 is closest to ERA5. Figure S9 shows that when using sfcWindmax, CORDEX
420 0.11 has heavier tails than CORDEX 0.44.

421
422 In summary, winds tend to be somewhat stronger, with somewhat heavier tails at higher resolution, with a large spread
423 between models. Reanalysis datasets give fairly diverse results.

424

425 **4.2 Global high resolution: UPSCALE**

426 We now examine the benefits or otherwise of global high vs. standard resolution simulations for simulating climate
427 extremes. Global high resolution may allow an improved representation of the large scale circulation that cannot be
428 captured by regional models, which may in turn affect the representation of climate extremes. For this we examine the

429 UPSCALE simulations (Mizielinski et al. 2014), which consist of a small ensemble of HadGEM3-A simulations at
430 three different resolutions: 130km (N96), 60km (N216), and 25km (N512) (see Data section).

431 **4.2.1 Temperature extremes**

432 Figure 5 shows the ensemble mean climatological mean of TXx5day for the UPSCALE simulations over the period
433 1985-2011 at all three resolutions, and their biases relative to E-OBS. The same general pattern of hotter extremes in
434 the south and colder in the north and over mountainous regions can be seen at all three resolutions, but temperature
435 extremes are hotter at higher resolution in the south and east, and colder over mountains. The same pattern of biases is
436 seen as for CORDEX and CMIP5 with cold biases in the north and hot in the south-east and over mountains. The
437 mountain biases reduce with higher resolution, as the orography becomes better defined, whilst the hot bias in the SE
438 and SW increases and the northern cold bias improves slightly. A coastal cold bias at low resolution disappears at
439 higher resolution as the model land mask becomes more detailed. Note that the SSTs are prescribed and are the same
440 for all simulations. Results for TXx are similar but hotter (not shown).

441
442 Figure 6 (left column) shows regional return period plots for TXx5day for the UPSCALE simulations. Results are a
443 little less consistent across regions for UPSCALE compared to the CMIP5 vs CORDEX analysis, so we split Northern
444 Europe into the British Isles and Scandinavia, and add the Alps, to better capture regional variations. Since the
445 ensemble means are only based on one model, results are presented without adjusting according to the climatology of
446 TXx5day, although such adjusted results can be seen in Figure S10 and allow differences in the shapes of the tails to
447 be seen more clearly. TXx5day seems to be somewhat hotter with higher resolution over many regions, although this
448 is not always clear cut. The Alps are a notable exception, where the higher elevations with higher resolution give rise
449 to colder temperature extremes. There are notable biases relative to E-OBS, with the models being too cold in the
450 north, especially at low resolution, whilst in the south the colder subset of models (N96, the lowest UPSCALE
451 resolution) agree best with the E-OBS. Over the Alps, again the low resolution simulations agree best with E-OBS,
452 with the warmest temperatures, but this will depend on the height of the meteorological stations. This apparent
453 contradiction to the reduced orographic hot bias with resolution in Figure 5 comes from the stronger cold bias of the
454 surrounding areas at low resolution. Figure S10 shows that differences between the shape of the tails with resolution
455 are not systematic across regions and are mostly small, whilst agreement with E-OBS is good everywhere. Results for
456 TXx are similar.

457
458 In summary, hot biases of temperature extremes over mountains reduce with increased resolution for HadGEM3-A.
459 Elsewhere extremes tend towards getting hotter with resolution, whilst the shapes of the return period curves are
460 insensitive.

461 **4.2.2 Precipitation extremes**

462 For precipitation, Figure 7 shows the ensemble mean climatological mean of Rx1day for the period 1989-2010 for the
463 three UPSCALE ensembles and their differences relative to E-OBS and MESAN. The overall pattern of Rx1day in the

464 simulations is similar to that in the observational datasets, with heavier precipitation extremes and finer spatial detail
465 with increasing resolution over complex orography. All resolutions have bands of heavy precipitation either side of
466 the Alps, but these move closer together as the Alps become better defined. All simulations are generally wetter than
467 E-OBS across most of Europe. The dry bias over orography in the Alps, Southern Norway and Scottish Highlands
468 reduces with resolution, whilst a wet bias on the southern edge of the Alps and the coastal side of the Dinaric Alps in
469 the Balkans appears instead. Comparing to MESAN instead of E-OBS, the general wet bias disappears, and the dry
470 mountain bias over orography at low resolution increases. The differences between resolutions appear smaller than for
471 the CMIP5 versus CORDEX analysis: all the UPSCALE simulations look most similar to CORDEX at 0.44° .
472 However, UPSCALE does not reach as fine a resolution as CORDEX at 0.11° (25 km vs 12.5 km), and CMIP5 is on
473 average slightly coarser than the N96 simulations. In addition, it should be noted that models with the same nominal
474 resolution do not necessarily have the same effective resolution, and that the effective resolution is always less than
475 the nominal resolution (Skamarock 2004; Klavar et al. 2020). Results are similar for Rx5day (not shown).

476
477 Figure 6 (middle column) shows the return period plots for Rx1day for the three resolutions of UPSCALE ensembles.
478 Slightly heavier precipitation extremes are found at higher resolution in all the regions shown (exceptions are France
479 and Mid Europe- not shown). Although the differences are small, they are more obvious in southern Europe and
480 especially in the Alps. Figure S10 shows that there is not much difference in the shape of the tails for most regions,
481 although there are very slightly heavier tails at higher resolution for southern Europe (more so in the Mediterranean
482 sub region- not shown) and more obvious differences over the Alps in the same direction, both of which are regions
483 where convective precipitation is important. E-OBS tends to lie just below the model simulations for most regions
484 (Figure 6), although it agrees with the models for the British Isles, and is between the low and medium resolution
485 simulations over the Alps. MESAN gives higher values for observed Rx1day which improves agreement in regions
486 where E-OBS lay below the models, and causes a higher resolution subset to agree better in the other regions (Figure
487 6). For the curves that are adjusted to have the same climatological mean, E-OBS tends to lie just on the lower end of
488 the ensemble for most regions, whilst MESAN gives slightly heavier tails and tends to improve agreement with models
489 (Figure S10). Results for Rx5day are broadly similar (except that both observational datasets lie above all the models
490 for the British Isles).

491
492 In summary, precipitation extremes are somewhat wetter and heavier tailed with increasing resolution mostly in
493 southern Europe and the Alps for HadGEM3-A. Dry orographic biases decrease with resolution, but wet biases appear
494 in the south next to mountain ranges instead.

495 **4.2.3 Wind extremes**

496 For wind extremes, Figure 8 shows the spatial patterns of climatological mean annual maximum wind for UPSCALE
497 and the same for three reanalyses. The spatial patterns are similar for the three different model resolutions, with the
498 highest winds over the British Isles and coastal regions, lower wind speeds over the Alps, and the zonal tripole pattern
499 described above. The main differences are that the lower resolution model (N96) has stronger winds around the British

500 Isles and western coastlines. This is likely because the larger coastal grid boxes overlap more with the ocean, which
501 tends to have higher wind speeds, or due to differences in the model land mask itself with resolution. The wind speeds
502 at higher resolution are a little stronger overall, most obviously in the central European zonal belt, and over the Alps
503 and Norwegian mountains. All resolutions show stronger winds than ERA5 over most of Europe. Compared to
504 MESCAN winds are too weak in the northern and southern Europe, particularly over mountainous regions, and a little
505 too strong in between. Relative to DYNAD the pattern of differences is similar as for MESCAN, but with stronger
506 negative differences over the Norwegian mountains and positive differences in other parts of Northern Europe. There
507 are positive coastal biases relative to all reanalyses for the N96 simulations that reduce with increased resolution.

508
509
510 Figure 6 (right column) shows the return period plots for some example regions for annual maximum wind for the
511 UPSCALE simulations, without shifting the climatology. Over all regions examined (except the Mediterranean- not
512 shown), the N512 simulations have stronger winds than the N216 simulations. The position of the curve for N96 is
513 strongly related to how much coastline there is relative to land area per region, e.g. with faster winds than the other
514 simulations over the British Isles and southern Europe, but relatively slower winds over central Europe, and particularly
515 over the Alps. There are fairly large differences between reanalysis estimates, with ERA5 always having the slowest
516 winds, and the model simulations tending to lie between ERA5 and the other two reanalyses for most regions. For the
517 adjusted versions of the return period plots (Figure S10), differences in the shapes of the tails with resolution are
518 generally small, although with marginally heavier tails with increasing resolution over a number of regions, e.g. the
519 Alps (not all are shown). MESCAN and DYNAD have slightly heavier tails than ERA5, particularly over the Alps and
520 Southern Europe. The shape of the model curves agree well with all reanalyses over the British Isles, Scandinavia and
521 Central Europe, and lie between ERA5 and the other two reanalyses for the Alps and Southern Europe.

522
523 In summary winds are slightly stronger and heavier tailed at higher resolution in HadGEM3-A, except over coastal
524 areas where large coastal grid boxes at low resolution bring strong ocean winds further over land.

525 **4.3 Upscaling versus downscaling**

526 For the global model results, any differences in the representation of extremes according to resolution could come from
527 either upscaling or downscaling effects. Upscaling effects could include a better representation of the large scale
528 circulation, whilst downscaling allows a better representation of small scale processes, such as convection, and an
529 improved representation of orography and coastlines. In order to investigate which of these effects leads to the
530 differences between the low (N96) and high resolution (N512) HadGEM3-A simulations, we employ a circulation
531 analogue technique (e.g. Vautard et al., 2016), which is frequently used in attribution studies (see e.g. Stott et al., 2016;
532 Cattiaux et al., 2010). The idea is to determine whether the simulation of climate extremes changes between the two
533 resolutions if both were to have the same large scale circulation –i.e. isolating the downscaling effect, or conversely
534 whether circulation differences explain any differences in extreme events whilst circulation-variable (e.g. precipitation)
535 relationships stay the same –i.e. the upscaling effect.

536
537 For each day in the lower resolution simulations we pick the nearest circulation analogue from anywhere in the higher
538 resolution simulations, providing it happens at the right time of year (i.e. within a 30-day window centred on the day
539 of the year in question). We then record the associated temperature, precipitation and wind values from the higher
540 resolution simulations to make a “*u*-chronic” dataset (e.g. Jézéquel, et al. 2018) that contains data from the high
541 resolution simulations but follows the daily sequence of circulation patterns from the low resolution models. We then
542 repeat the analysis of return periods and value as above. We also do the reverse (find analogues for the N512 circulation
543 in the N96 ensemble and record the N96 temperature). Since results using analogues are not directly comparable to the
544 original results due to the lack of an exact analogue match, we also perform “self-analogues” -i.e. finding circulation
545 analogues for the N96 simulations within the N96 ensemble, (excluding the same year from the same ensemble
546 member) and creating a *u*-chronic time series, and the same for the N512 ensemble). Comparing the resulting return
547 period curves tells us about the contribution of large-scale circulation and downscaling to differences in extremes
548 between the two resolutions. For example, comparing the N96 self-analogue return curve to the version based on N512
549 circulation but with N96 precipitation shows us the contribution of any differences in the large scale circulation
550 between the resolutions i.e. the upscaling effect. Comparing the N96 self-analogue to the version based on N96
551 circulation with N512 precipitation shows us the downscaling effect – i.e. any difference between the relationship
552 between the large scale circulation and precipitation.

553
554 Analogues are defined using geopotential height at 500 hPa, since this avoids complications relating to surface heat
555 lows associated with heat waves in anticyclonic conditions that occur in summer, whilst also avoiding incomplete data
556 due to mountain ranges. Geopotential height is regridded to a 2° grid using bilinear interpolation. This choice ensures
557 that we are comparing analogues with the same resolution and do not penalise small-scale differences. Similarity
558 between circulation states is quantified using pattern correlation, which is not affected by trends in geopotential height
559 with global warming. For precipitation and wind the European domain used is -16 to 44° E and 34 to 72° N (roughly
560 the same as the domain plotted in the map-based figures). For temperature, a larger domain is used, since the history
561 and trajectory of air masses are important for temperature extremes. This domain is loosely based on the domain used
562 by Cattiaux et al. (2010) and extends over the N. Atlantic as well as Europe, (-62 to 44°E and 24 to 80° N). However,
563 results are very similar if the smaller domain is used (not shown). For the 5-day variables (Rx5day and TXx5day) the
564 *u*-chronic dataset was smoothed using a 5-day running mean. We also tried smoothing the daily geopotential height,
565 precipitation and temperature datasets first and then performing the analogue analysis. The relationship between the
566 different curves was largely consistent between the two approaches, but absolute values differed and the shape of the
567 curves changed a little. Results presented here are based on the first approach.

568
569 Figure 9 shows the results of the analogue analysis. The blue curves show the results for the N512 self-analogues, grey
570 represents the N96 self-analogues, red represents results using the circulation patterns from the N96 runs but with the
571 N512 circulation-variable relationships, and green indicates N512 circulation with N96 circulation-variable
572 relationships. The difference between the blue and red curves (or the grey and green curves) shows the contribution

573 from differences in the large scale circulation with resolution, whilst the difference between the blue and green curves
574 (or the red and grey curves) indicates the downscaling effect.

575
576 For Txx5day downscaling effects are dominant over regions that have a clear difference between resolutions, although
577 circulation differences also have a small effect in some regions such as the British Isles (Figure 9). For Rx1day the
578 different curves are very close together for some regions, making it difficult to discern the relative contributions from
579 upscaling and downscaling. However, for regions with an obvious difference between resolutions, such as the Alps
580 and Southern Europe, downscaling effects seem to be the most important. Interestingly, these are regions where
581 convective precipitation is particularly important for precipitation extremes. For wind extremes downscaling effects
582 also dominate, particularly over the British Isles, central Europe and the Alps. Results for Txx and Rx5day are very
583 similar to those for Txx5day and Rx1day respectively (not shown).

584
585 Also shown, using dashed lines, are the original ensemble mean results without using analogues. By comparing these
586 with the self-analogue results we can see how successful the analogue technique is in recreating the original
587 distributions. The self-analogue results tend to be close to the original results for wind and Rx1day, but below them
588 for Tx5day. Undertaking the 5-day smoothing first rather than last (see above) shifts analogue results upwards, above
589 the original curves, but the other aspects of the results are the same (not shown). A similar phenomenon is seen for
590 Rx5day (not shown).

591
592 In summary, for all three types of extreme events, downscaling effects appear to dominate the differences seen between
593 the 130km and 25km HadGEM3-A simulations. This suggests that at least for this model, any large scale circulation
594 differences obtained with global high resolution do not affect the statistics of these extreme events much.

595 **5 Discussion and Conclusions**

596 We evaluated climate model simulations of temperature, precipitation and wind extremes over Europe, addressing
597 three questions: 1) The benefits of dynamical downscaling using regional climate models by comparing EURO-
598 CORDEX simulations at two resolutions (12.5 and 50 km) to their driving coarser resolution CMIP5 models; 2) The
599 benefits of increased resolution for global models by comparing HadGEM3-A simulations at three resolutions (130,
600 60 and 25 km; referred to as the “UPSCALE” simulations); and 3) whether any differences according to resolution in
601 the global model comes from differences in the large scale circulation (upscaling) or the representation of small scale
602 processes, and features (downscaling) using a circulation analogue method.

603
604 For temperature extremes, increased resolution did not make much difference to results for the CORDEX vs CMIP5
605 analysis in terms of the shapes of the return period curves, which all agreed well with observational data. Hot biases
606 over mountains reduced with increased resolution, although the cold bias over Scandinavia was worse in CORDEX
607 than in CMIP5. This amplified Scandinavian cold bias in CORDEX is consistent with the findings of Sørland et al
608 (2018) for mean summer temperature, although we did not find the same reduction of the warm bias in Eastern Europe

609 in CORDEX as they did, possibly due to differences in the models used. Our findings agree with Vautard et al. (2013),
610 who find limited benefits in simulating various aspects of heatwaves between the 0.44° and 0.11° versions of the
611 EURO-CORDEX models. The reduction in orographic bias with increased resolution was also seen in the HadGEM3-
612 A GCM simulations, along with a general tendency towards hotter extremes elsewhere, which reduces biases in the
613 north, and increases them in the south. Overall the benefits of increasing resolution were limited, or region dependent.
614 However, our results for the global model analysis are based on only one model and the new model simulations and
615 analyses being generated as part of the PRIMAVERA and HighResMIP projects (<https://www.primavera-h2020.eu/>;
616 Roberts et al. 2018; Haarsma et al. 2016) will be very useful for determining how representative our results for
617 HadGEM3-A are of other GCMs. For instance, improvements in the simulation of summer blocking, which can be
618 involved in heatwave generation is very model dependent (Schiemann et al. 2014). Furthermore, Cattiaux et al. (2013)
619 find that the frequency, intensity and duration of summer heatwaves improve in the IPSL model with resolution,
620 associated with a better representation of the large scale circulation. In addition, here we examine only one aspect of
621 heat waves (intensity), and it could be that results are different for other aspects, such as frequency, duration and
622 timing.

623
624 Precipitation extremes were more sensitive to resolution, particularly in the CMIP5 vs CORDEX analysis, with heavier
625 tails at higher resolution across all regions. Spatially, CMIP5 shows a general dry bias compared to E-OBS, particularly
626 over mountainous regions, whilst CORDEX shows the opposite, with increasing wet differences at 0.11° compared to
627 0.44°, which appears to be systematic across models. This is consistent with results for mean precipitation in EURO-
628 CORDEX in Kotlarski et al. (2014). The higher resolution MESAN reanalysis gave wetter extremes and heavier tails
629 than E-OBS, agreeing best with the 0.44° resolution CORDEX simulations. Other studies suggest that country-scale
630 higher resolution precipitation datasets give heavier precipitation extremes still, which may agree best with the 0.11°
631 simulations (e.g. Prein and Gobiet 2017). Similarly, for mean precipitation, Prein and Gobeit (2017) find that RCM
632 biases are a similar size to the differences between different observational estimates. For extreme precipitation, various
633 studies find that a number of aspects (biases, frequency-intensity distributions, spatial patterns) of mean and extreme
634 precipitation improve in EURO-CORDEX at 0.11° compared to 0.44° when compared to such high resolution datasets
635 (e.g. Prein et al. 2016; Torma et al. 2015; Fantini et al. 2020). Prein et al (2016) ascribe this mostly to the better
636 representation of orography at higher resolution, but also the ability to capture the larger scales of convection.
637 However, aside from improved spatial patterns Casanueva et al (2016) found only limited evidence for improvements
638 in precipitation intensity, frequency and derived indicators over the Alps and Spain with resolution in EURO-
639 CORDEX. Some of the differences with resolution in our results may also be explained by parameterisation schemes
640 that tend to be tuned to one resolution and can behave sub-optimally at others.

641
642 For the UPSCALE global simulations, there was less difference in extreme precipitation with resolution, with the
643 biggest differences in southern regions or over or near mountains, with heavier tails and wetter extremes at higher
644 resolution. This reduced dry biases over orography, but wet biases next to some mountain ranges in the south emerged
645 instead. However, these simulations span a narrower range of resolutions, i.e. not reaching the same high resolutions
646 as CORDEX 0.11°, but also not as coarse as some CMIP5 models. Other global model studies also tend to find an

647 increase in precipitation extremes with increased resolution for Europe, which is continent-wide in summer, and
648 concentrated in mountainous regions in winter (Volosciuk et al. 2015; Wehner et al. 2014). This sometimes improves
649 agreement with observational data (e.g. Kopparla et al. 2013; Wehner et al. 2014 for winter), but can overestimate
650 summer extreme precipitation if parameterisation schemes are not retuned (Wehner et al. 2014).

651
652 For wind extremes, higher resolution gave somewhat stronger winds and heavier tails for most regions for both the
653 CORDEX vs CMIP5 analysis and to a lesser extent for HadGEM3-A, except for regions dominated by coasts for the
654 latter, where large coastal grid boxes at lower resolution brought strong ocean winds further over land. Stronger winds
655 with higher resolution are also found in previous studies (e.g. Pryor et al. 2012; Kunz et al. 2010; Gao et al. 2020). The
656 largest differences we found were between CMIP5 and CORDEX at 0.44°, with less difference between the two
657 resolutions of CORDEX. Differences between reanalysis-based estimates made model evaluation difficult.

658
659 The results of the circulation analogue analysis on the HadGEM3-A GCM simulations suggested that downscaling
660 effects were the dominant cause of differences with resolution for all three phenomena, with limited effects of any
661 differences in the representation of the large scale circulation. If this result also applied to other GCMs, it would suggest
662 that dynamical downscaling with more economical limited area models would be a better strategy for simulating
663 European extreme events, whilst GCM efforts could focus on other aspects such as multiple members or multi-physics
664 ensembles. However, we cannot reach this conclusion based solely on this analysis, since we examine only a single
665 model, which may not be representative of other models, and because the range of resolutions considered may be too
666 narrow. Demory et al. (2020) and Strandberg and Lind (2020) found that PRIMAVERA GCM simulations and EURO-
667 CORDEX simulations at comparable resolution simulated fairly similar precipitation PDFs to each other, which would
668 agree with a limited influence of upscaling. However, a number of studies do find improvements in the large-scale
669 circulation with resolution, including for extra-tropical cyclones and storm tracks (Colle et al. 2013; Jung et al 2006;
670 2012, Zappa et al. 2013), Euro-Atlantic weather regimes (Dawson et al. 2012; 2015; Cattiaux et al. 2013; Strommen
671 et al. 2019; Fabiano et al. 2020) and blocking (Jung et al. 2012, Anstey et al. 2013; Matsueda et al. 2009, Berckmans
672 et al 2013; Schiemann et al. 2017; 2020; Davini et al 2017a; 2017b; 2020; see also Introduction). Interestingly,
673 Schiemann et al. (2017) find improvements in Euro-Atlantic blocking with resolution in all seasons in the same
674 HadGEM3-A simulations as we analyse here. However, the net effects on extremes, given all uncertainties, was not
675 explicitly investigated. Our study does not seem to be able to discern such effects. Other studies suggest that benefits
676 from upscaling may require convective permitting simulations (Hart et al. 2018).

677
678 Overall our results suggest that whether or not increased resolution is beneficial for the simulation of extreme events
679 over Europe depends on the event being considered. Benefits appear limited for heatwaves, whereas wind extremes
680 and particularly precipitation extremes are more sensitive. We do not find any particular advantage in using a global
681 high resolution model compared to regional dynamical downscaling, with the caveats that this investigation needs to
682 be extended to other GCMs, and a wider range of resolutions should be investigated.

683

684 In order to fully address the question of the benefits of increased resolution for European climate extremes, a number
685 of aspects remain to be investigated. Firstly, the analysis could be widened to other types of extremes, for example,
686 sea level rise and storm surge, or other aspects of extremes could be considered e.g. timing, frequency and duration of
687 events. The global simulations we investigated were atmosphere-only, and the role of increased ocean resolution and
688 also vertical resolution and model top height should be considered. Finally, we assume that better historical
689 performance translates into more accurate future projections. Lhotka et al. (2018) find low sensitivity of heatwave
690 projections to resolution in EURO-CORDEX RCMs. However, Van Haren et al. (2015b) and van der Linden et al.
691 (2019) find stronger future summer drying and heating in central Europe with increased resolution in the EC-Earth
692 GCM due to differences in atmospheric circulation. Concerning precipitation, future projections for large scale and
693 seasonal mean precipitation are consistent between large scale regional and convective permitting models, whilst there
694 is evidence that summer sub-daily intensities increase more in the future in convection permitting models (Kendon et
695 al. 2014; 2017; Ban et al. 2015). For wind, Willison et al. (2015) find a larger response of the North Atlantic storm
696 track to global warming with higher resolution in the regional WRF model. Furthermore, Baker et al. (2019) find that
697 in winter the polar jet, storm tracks and associated precipitation shift further North over the Euro-Atlantic region in the
698 future with increased resolution in the same HadGEM3-A set up as used here. The sensitivity of projections to
699 resolution nevertheless remains an area that needs further research.

700
701 Finally, ongoing projects such as HighResMIP for CMIP6 (Haarsma et al., 2016), and the CORDEX Flagship Pilot
702 Studies, particularly the FPS on Convective Phenomena at High Resolution over Europe and the Mediterranean
703 (Coppola et al., 2019; Jacob et al 2020), will enable the benefits of high resolution and its effect on European climate
704 projections to be explored more thoroughly. The former will allow a systematic exploration of the effects of increased
705 resolution for multiple GCMs through coordinated experiments simulating the past and future climate. The latter will
706 include a first of its kind large multi-model ensemble at convective permitting resolution for decadal time slices in the
707 present and future for a large domain covering central Europe and part of the Mediterranean.

708 **Data and code availability**

709 The CMIP5 and CORDEX data used for this analysis are available from the Earth System Grid Federation portals, and
710 are detailed in Table S1. The HadGEM3-A UPSCALE simulations are available from the CEDA-JASMIN platform.
711 E-OBS can be downloaded here <https://www.ecad.eu/download/ensembles/download.php>, MESAN is available here
712 <http://exporter.nsc.liu.se/620eed0cb2c74c859f7d6db81742e114/>, ERA5 and MESCAN are available from the
713 Copernicus Climate Data Store <https://cds.climate.copernicus.eu>, whilst DYNAD winds are available from Tomas
714 Landelius at SMHI.

715 **Author contributions**

716 CI, RV and SJ conceptualised the study, CI carried out the analysis and wrote the manuscript, JS managed the CRECP
717 project together with CH and BE, and all co-authors were involved in discussions to prepare the study and helped
718 improve the manuscript.

719 **Competing interests**

720 The authors declare that they have no conflict of interest.

721 **Acknowledgements**

722 This work is published in the name of the European Commission, with funding from the European Union through the
723 Copernicus Climate Change Service project C3S_34a Lot 3 (Copernicus Roadmap for European Climate Projections).
724 The Commission is not responsible for any use that may be made of the information contained. We acknowledge the
725 WCRP's Working Group on Regional Climate, and the Working Group on Coupled Modelling - the coordinating body
726 of CORDEX and the panel responsible for CMIP5 respectively. We thank the climate modelling groups for producing
727 and making available the model output listed in Supplementary Table 1, which is available at <http://pcmdi9.llnl.gov>.
728 For CMIP, the US Department of Energy's Program for Climate Model Diagnosis and Intercomparison provides
729 coordinating support and led development of software infrastructure in partnership with the Global Organization for
730 Earth System Science Portals. We thank the modelling team that produced the UPSCALE simulations, and
731 acknowledge the JASMIN and IPSL mesocentre computing clusters on which this analysis was performed. We thank
732 Tomas Landelius from SMHI for making the DYNAD wind data available. We also acknowledge helpful input from
733 the CRECP project scientific advisory board and useful discussions with UK Met Office Scientists, in particular
734 Malcolm Roberts and Carol McSweeney. We thank four anonymous reviewers for their helpful comments and
735 suggestions.

736

737 **References**

738 Anstey, J. A., Davini, P., Gray, L. J., Woollings, T. J., Butchart, N., Cagnazzo, C., Christiansen, B., Hardiman, S. C.,
739 Osprey, S. M. and Yang, S.: Multi-model analysis of Northern Hemisphere winter blocking: Model biases and the role
740 of resolution, *J. Geophys. Res. Atmos.*, 118, 3956–3971, doi: 10.1002/jgrd.50231, 2013.

741
742 Bador, M., Boé, J., Terray, L., Alexander, L. V., Baker, A., Bellucci, A., Haarsma, R., Koenigk, T., Moine, M-P.,
743 Lohmann, K., Putrasahan, D. A., Roberts, C., Roberts, M., Scoccimarro, E., Schiemann, R., Seddon, J., Senan, R.,
744 Valcke, S., and Vanniere, B.: Impact of higher spatial atmospheric resolution on precipitation extremes over land in
745 global climate models. *J. Geophys. Res. Atmos.*, 125, e2019JD032184. <https://doi.org/10.1029/2019JD032184>, 2020

746

747 Baker, A.J., Schiemann, R., Hodges, K. I., Demory, M., Mizielinski, M. S., Roberts, M. J., Shaffrey, L. C., Strachan,
748 J. and Vidale, P. L.: Enhanced Climate Change Response of Wintertime North Atlantic Circulation, Cyclonic Activity,
749 and Precipitation in a 25-km-Resolution Global Atmospheric Model. *J. Climate*, 32, 7763–7781, [https://doi-](https://doi-org.ezproxy.is.ed.ac.uk/10.1175/JCLI-D-19-0054.1)
750 [org.ezproxy.is.ed.ac.uk/10.1175/JCLI-D-19-0054.1](https://doi-org.ezproxy.is.ed.ac.uk/10.1175/JCLI-D-19-0054.1), 2019

751

752 Ban, N., Schmidli, J. and Schär, C.: Heavy precipitation in a changing climate: Does short-term summer precipitation
753 increase faster?, *Geophys. Res. Lett.*, 42, 1165–1172, doi: 10.1002/2014GL062588, 2015.

754

755 Bazile, E., Abida, R., Verrelle, A., Le Moigne, P. and Szczypta, C. : Report for the 55years MESCAN-SURFEX re-
756 analysis, deliverable D2.8of the UERRA project, pp. 22, available from: [http://www.uerra.eu/publications/deliverable-](http://www.uerra.eu/publications/deliverable-reports.html)
757 [reports.html](http://www.uerra.eu/publications/deliverable-reports.html), 2017

758

759 Berckmans, J., Woollings, T., Demory, M. E., Vidale, P.-L. and Roberts, M.: Atmospheric blocking in a high resolution
760 climate model: influences of mean state, orography and eddy forcing, *Atmos. Sci. Lett.*, 14, 34–40,
761 doi:10.1002/asl2.412, 2013.

762

763 Casanueva, A., Kotlarski, S., Herrera, S., Fernández, J., Gutiérrez, J.M., Boberg, F., Colette, A., Christensen, O. B.,
764 Goergen, K., Jacob, D., Keuler, K., Nikulin, G., Teichmann C. and Vautard, R.: Daily precipitation statistics in a
765 EURO-CORDEX RCM ensemble: added value of raw and bias-corrected high-resolution simulations, *Clim Dynam*,
766 47,719-737. <https://doi.org/10.1007/s00382-015-2865-x>, 2016

767

768 Cattiaux, J., Vautard, R., Cassou, C., Yiou, P., Masson-Delmotte, V., and Codron, F.: Winter 2010 in Europe: A cold
769 extreme in a warming climate, *Geophys. Res. Lett.*, 37, L20704, doi: 10.1029/2010GL044613, 2010.

770

771 Cattiaux, J., Quesada, B., Arakélian, A., Codron, F., Vautard, R., Yiou, P.: North-Atlantic dynamics and European
772 temperature extremes in the IPSL model: sensitivity to atmospheric resolution, *Clim. Dynam.*, 40, 2293-2310,
773 doi:10.1007/s00382-012-1529-3, 2013.

774

775 Christensen, J. H. and Christensen, O. B.: A summary of the PRUDENCE model projections of changes in European
776 climate by the end of this century, *Climatic Change*, 81, 7–30, doi: 10.1007/s10584-006-9210-7, 2007.

777

778 Colle, B. A., Zhang, Z., Lombardo, K., Liu, P., Chang, E. and Zhang, M.: Historical evaluation and future prediction
779 in Eastern North America and western Atlantic extratropical cyclones in the CMIP5 models during the cool season, *J.*
780 *Climate.*, 26, 882–903, doi: 10.1175/JCLI-D-12-00498.1, 2013.

781

782 Coppola, E., Sobolowski, S., Pichelli, E., Raffaele, F., Ahrens, B., Anders, I., Ban, N., Bastin, S., Belda, M., Belusic,
783 D., Caldas-Alvarez, A., Margarida Cardos, R., Davolio, S., Dobler, A., Fernandez, J., Fita Borrell, L., Fumiere, Q.,

784 Giorgi, F., Goergen, K., Guettler, I., Halenka, T., Heinzeller, D., Hodnebrog, Ø., Jacob, D., Kartsios, S., Katragko, E.,
785 Kendon, E., Khodayar, S., Kunstmann, H., Knist, S., Lavín, A., Lind, P., Lorenz, T., Maraun, D., Marelle, L., van
786 Meijgaard, E., Milovac, J., Myhre, G., Panitz, H.-J., Piazza, M., Raffa, M., Raub, T., Rockel, B., Schär, C., Sieck, K.,
787 Soares, P. M. M., Somot, S., Srnec, L., Stocchi, P., Tölle, M., Truhetz, H., Vautard, R., de Vries, H. and Warrach-Sagi,
788 K.: A first-of-its-kind multi-model convection permitting ensemble for investigating convective phenomena over
789 Europe and the Mediterranean, *Clim. Dynam.*, 1-32, <https://doi.org/10.1007/s00382-018-4521-8>, 2018.

790

791 Dahlgren, P., Landelius, T., Kållberg, P. and Gollvik, S., A high-resolution regional reanalysis for Europe. Part 1:
792 Three-dimensional reanalysis with the regional High-Resolution Limited-Area Model (HIRLAM), *Q.J.R. Meteorol.*
793 *Soc.*, 142, 2119-2131, doi:10.1002/qj.2807, 2016

794

795 Davini, P., Corti, S., D'Andrea, F., Rivière, G., and von Hardenberg, J.: Improved Winter European Atmospheric
796 Blocking Frequencies in High-Resolution Global Climate Simulations. *J. Adv. Model. Earth Syst.*, 9, 2615–2634,
797 <https://doi.org/10.1002/2017MS001082>, 2017a.

798

799 Davini, P., von Hardenberg, J., Corti, S., Christensen, H. M., Juricke, S., Subramanian, A., Watson, P. A. G.,
800 Weisheimer, A., and Palmer, T. N.: Climate SPHINX: evaluating the impact of resolution and stochastic physics
801 parameterisations in the EC-Earth global climate model, *Geosci. Model Dev.*, 10, 1383-1402,
802 <https://doi.org/10.5194/gmd-10-1383-2017>, 2017b.

803

804 Davini, P., and D'Andrea, F.: From CMIP-3 to CMIP-6: Northern Hemisphere atmospheric blocking simulation in
805 present and future climate. *J. Climate*, doi: <https://doi.org/10.1175/JCLI-D-19-0862.1>, 2020

806

807 Dawson, A. and Palmer, T. N.: Simulating weather regimes: impact of model resolution and stochastic
808 parameterization. *Clim Dynam*, 44, 2177-2193, <https://doi.org/10.1007/s00382-014-2238-x>, 2015.

809

810 Dawson, A., Palmer, T. N., and Corti, S.: Simulating regime structures in weather and climate prediction models,
811 *Geophys. Res. Lett*, 39, L21805, <https://doi.org/10.1029/2012GL053284>, 2012.

812

813 Dee, D. P., Uppala, S. M., Simmons, A. J, Berrisford, P., Poli, P., Kobayashi, S., Andrae, U., Balmaseda, M. A.,
814 Balsamo, G., Bauer, P., Bechtold, P., Beljaars, A. C., van de Berg, L., Bidlot, J., Bormann, N., Delsol, C., Dragani, R.,
815 Fuentes, M., Geer, A. J., Haimberger, L., Healy, S. B., Hersbach, H., Hólm, E. V., Isaksen, L., Kållberg, P., Köhler,
816 M., Matricardi, M., McNally, A. P., Monge-Sanz, B. M., Morcrette, J., Park, B., Peubey, C., de Rosnay, P., Tavolato,
817 C., Thépaut, J. and Vitart, F.: The ERA-Interim reanalysis: Configuration and performance of the data assimilation
818 system, *Q. J. R. Meteorol. Soc.*, 137, 553–597, <https://doi.org/10.1002/qj.828>, 2011.

819

820 Demory, M. E., Vidale, P. L., Roberts, M. J., Berrisford, P., Strachan, J., Schiemann, R., and Mizielinski, M. S.: The
821 role of horizontal resolution in simulating drivers of the global hydrological cycle, *Clim. Dynam.*, 42, 2201–2225,
822 <https://doi.org/10.1007/s00382-013-1924-4>, 2014.

823

824 Demory, M.-E., Berthou, S., Sørland, S. L., Roberts, M. J., Beyerle, U., Seddon, J., Haarsma, R., Schär, C.,
825 Christensen, O. B., Fealy, R., Fernandez, J., Nikulin, G., Peano, D., Putrasahan, D., Roberts, C. D., Steger, C.,
826 Teichmann, C., and Vautard, R.: Can high-resolution GCMs reach the level of information provided by 12–50 km
827 CORDEX RCMs in terms of daily precipitation distribution?, *Geosci. Model Dev. Discuss.*,
828 <https://doi.org/10.5194/gmd-2019-370>, in review, 2020.

829

830 Donat M. G., Leckebusch G. C., Wild S., Ulbrich U.: Benefits and limitations of regional multi-model ensembles for
831 storm loss estimations, *Clim. Res.*, 44, 211–225. <https://doi.org/10.3354/cr00891>, 2010.

832

833 Donlon, C. J., Martin, M., Stark, J., Roberts-Jones, J., Fiedler, E., and Wimmer, W.: The Operational Sea Surface
834 Temperature and Sea Ice Analysis (OSTIA) system, *Remote Sens. Environ.*, 116, 140–158,
835 [doi:10.1016/j.rse.2010.10.017](https://doi.org/10.1016/j.rse.2010.10.017), 2012.

836

837 Eyring, V., Bony, S., Meehl, G. A., Senior, C. A., Stevens, B., Stouffer, R. J., and Taylor, K. E.: Overview of the
838 Coupled Model Intercomparison Project Phase 6 (CMIP6) experimental design and organization, *Geosci. Model Dev.*,
839 9, 1937–1958, <https://doi.org/10.5194/gmd-9-1937-2016>, 2016.

840

841 Fabiano, F., Christensen, H.M., Strommen, K., Athanasiadis, P., Baker, A., Schiemann, R. and Corti, S: Euro-Atlantic
842 weather Regimes in the PRIMAVERA coupled climate simulations: impact of resolution and mean state biases on
843 model performance. *Clim Dyn* 54, 5031–5048. <https://doi.org/10.1007/s00382-020-05271-w>, 2020

844

845 Fantini, A., Raffaele, F., Torma, C., Bacer, S., Coppola, E., Giorgi, F., Ahrens, B., Dubois, C., Sanchez, E. and
846 Verdecchia, M.: Assessment of multiple daily precipitation statistics in ERA-Interim driven Med-CORDEX and
847 EURO-CORDEX experiments against high resolution observations. *Clim Dyn* **51**, 877–900.
848 <https://doi.org/10.1007/s00382-016-3453-4>, 2018

849

850 Førland, E. and Institut, N. M.: Manual for Operational Correction of Nordic Precipitation Data. Norwegian
851 Meteorological Institute., 1996.

852

853 Gao, J., G., Shoshiro, M., Roberts, M. J., Haarsma, R., Putrasahan, D., Roberts, C. D., Scoccimarro, E., Terray, L.,
854 Vannière, B. and Vidale, P. L.: Influence of model resolution on bomb cyclones revealed by HighResMIP-
855 PRIMAVERA simulations, *Environ. Res. Lett.* 15, 084001, <https://doi.org/10.1088/1748-9326/ab88fa>, 2020

856

857 Giorgi F., Jones C., Asrar G. R.: Addressing climate information needs at the regional level: the CORDEX framework,
858 WMO Bull., 58:175–183, 2009.

859

860 Goodison, B. E., Louie, P. Y. and Yang, D.: The WMO solid precipitation measurement intercomparison. World
861 Meteorological Organization-Publications-WMO TD, Report No. 67, 65–70, 1997.

862

863 Gutjahr, O., Schefczyk, L., Reiter, P. and Heinemann, G.: Impact of the horizontal resolution on the simulation of
864 extremes in COSMO-CLM, Meteorol. Z., 25, 543 – 562, doi: 10.1127/metz/2016/0638, 2016.

865

866 Haarsma, R. J., Roberts, M. J., Vidale, P. L., Senior, C. A., Bellucci, A., Bao, Q., Chang, P., Corti, S., Fuckar, N. S.,
867 Guemas, V., von Hardenberg, J., Hazeleger, W., Kodama, C., Koenigk, T., Leung, L. R., Lu, J., Luo, J.-J., Mao, J.,
868 Mizielinski, M. S., Mizuta, R., Nobre, P., Satoh, M., Scoccimarro, E., Semmler, T., Small, J., and von Storch, J.-S.:
869 High Resolution Model Intercomparison Project (HighResMIP v1.0) for CMIP6, Geosci. Model Dev., 9, 4185-4208,
870 <https://doi.org/10.5194/gmd-9-4185-2016>, 2016.

871

872 Hart, N. C. G., Washington, R., and Stratton, R. A.: Stronger local overturning in convective-permitting regional
873 climate model improves simulation of the subtropical annual cycle. Geophys. Res. Lett., 45, 11334–11342,
874 <https://doi.org/10.1029/2018GL079563>, 2018.

875

876 Haylock, M. R., Hofstra, N., Klein Tank, A. M. G., Klok, E. J., Jones, P. D., New, M.: A European daily high-resolution
877 gridded data set of surface temperature and precipitation for 1950-2006. J. Geophys. Res. Atmos., 113, D20119.
878 doi:10.1029/2008JD010201, 2008.

879

880 Herrera, S., Cardoso, R. M., Soares, P. M., Espírito-Santo, F., Viterbo, P., and Gutiérrez, J. M.: Iberia01: a new gridded
881 dataset of daily precipitation and temperatures over Iberia, Earth Syst. Sci. Data, 11, 1947–1956,
882 <https://doi.org/10.5194/essd-11-1947-2019>, 2019.

883

884 Herrmann, M., Somot, S., Calmanti, S., Dubois, C., and Sevault, F.: Representation of spatial and temporal variability
885 of daily wind speed and of intense wind events over the Mediterranean Sea using dynamical downscaling: impact of
886 the regional climate model configuration, Nat. Hazards Earth Syst. Sci., 11, 1983-2001, [https://doi.org/10.5194/nhess-](https://doi.org/10.5194/nhess-11-1983-2011)
887 11-1983-2011, 2011.

888

889 Hersbach, H., Bell, B., Berrisford, P., Horányi, A., Muñoz-Sabater, J., Nicolas, J., Radu, R., Schepers, D., Simmons,
890 A., Soci, C., Dee, D.: Global reanalysis: goodbye ERA-Interim, hello ERA5. ECMWF, doi:10.21957/vf291hehd7.
891 <https://www.ecmwf.int/node/19027>, 2019

892

893 Jacob, D., Petersen, J., Eggert, B., Alias, A., Christensen, O. B., Bouwer, L. M., Braun, A., Colette, A., Déqué, M.,
894 Georgievski, G., Georgopoulou, E., Gobiet, A., Menut, L., Nikulin, G., Haensler, A., Hempelmann, N., Jones, C.,

895 Keuler, K., Ko-vats, S., Kröner, N., Kotlarski, S., Kriegsmann, A., Martin, E., Meijgaard, E. van, Moseley, C., Pfeifer,
896 S., Preuschmann, S., Radermacher, C., Radtke, K., Rechid, D., Rounsevell, M., Samuelsson, P., Somot, S., Soussana,
897 J.-F., Teichmann, C., Valentini, R., Vautard, R., Weber, B., and Yiou, P.: EURO-CORDEX: new high-resolution
898 climate change projections for European impact research, *Reg. Environ. Change*, 14, 563–578, doi:10.1007/s10113-
899 013-0499-2, 2014.

900

901 Jacob, D., Teichmann, C., Sobolowski, S. *et al.* Regional climate downscaling over Europe: perspectives from the
902 EURO-CORDEX community. *Reg Environ Change*, **20**, 51, <https://doi.org/10.1007/s10113-020-01606-9>, 2020

903

904 Jézéquel, A., Yiou, P. and Radanovics, S.: Role of circulation in European heatwaves using flow analogues. *Clim.*
905 *Dynam.* 50, 1145-1159, <https://doi.org/10.1007/s00382-017-3667-0>, 2018.

906

907 Jourdier, B.: Evaluation of ERA5, MERRA-2, COSMO-REA6, NEWA and AROME to simulate wind power
908 production over France, *Adv. Sci. Res.*, 17, 63–77, <https://doi.org/10.5194/asr-17-63-2020>, 2020.

909

910 Jung, T., Gulev, S. K., Rudeva, I. and Soloviov, V.: Sensitivity of extratropical cyclone characteristics to horizontal
911 resolution in the ECMWF model. *Q.J.R. Meteorol. Soc.*, 132, 1839-1857, doi:10.1256/qj.05.212, 2006.

912

913 Jung, T., Miller, M. J., Palmer, T. N., Towers, P., Wedi, N., Achuthavarier, D., Adams, J. M., Alshuler, E. L., Cash,
914 B. A., Kinter, J. L., Marx, L., Stan, C., and Hodges, K. I.: High-Resolution Global Climate Simulations with the
915 ECMWF Model in Project Athena: Experimental Design, Model Climate, and Seasonal Forecast Skill, *J. Climate.*, 25,
916 3155–3172, doi:10.1175/JCLI-D-11-00265.1, 2012.

917

918 Kendon, E. J., Roberts, N. M., Senior, C. A., and Roberts, M. J.: Realism of rainfall in a very high-resolution regional
919 climate model, *J. Climate.*, 25, 5791–5806. doi: 10.1175/JCLI-D-11-00562.1, 2012.

920

921 Kendon, E. J., Roberts, N. M., Fowler, H. J., Roberts, M. J., Chan, S. C., and Senior, C. A.: Heavier summer downpours
922 with climate change revealed by weather forecast resolution model, *Nat. Clim. Change*, 4, 570–576, doi:
923 10.1038/nclimate2258, 2014.

924

925 Kendon, E. J., Ban, N., Roberts, N. M., Fowler, H. J., Roberts, M. J., Chan, S. C., Evans, J. P., Fosser, G. and
926 Wilkinson, J.M.: Do Convection-Permitting Regional Climate Models Improve Projections of Future Precipitation
927 Change?. *B. Am. Meteorol. Soc.*, 98, 79–93, <https://doi.org/10.1175/BAMS-D-15-0004.1>, 2017.

928

929 Klaver, R., Haarsma, R., Vidale, P. L., Hazeleger, W.: Effective resolution in high resolution global atmospheric
930 models for climate studies. *Atmos Sci Lett.*, 1– 8. <https://doi.org/10.1002/asl.952>, 2020

931

932 Kopparla, P., Fischer, E. M., Hannay, C., and Knutti, R.: Improved simulation of extreme precipitation in a high-
933 resolution atmosphere model, *Geophys. Res. Lett.*, 40, 5803-5808, doi: 10.1002/2013GL057866, 2013.

934

935 Kotlarski, S., Keuler, K., Christensen, O. B., Colette, A., Déqué, M., Gobiet, A., Goergen, K., Jacob, D., Lüthi, D.,
936 van Meijgaard, E., Nikulin, G., Schär, C., Teichmann, C., Vautard, R., Warrach-Sagi, K., and Wulfmeyer, V.: Regional
937 climate modeling on European scales: a joint standard evaluation of the EURO-CORDEX RCM ensemble, *Geosci.*
938 *Model Dev.*, 7, 1297–1333, <https://doi.org/10.5194/gmd-7-1297-2014>, 2014.

939

940 Kunz, M., Mohr, S., Rauthe, M., Lux, R., and Kottmeier, C.: Assessment of extreme wind speeds from Regional
941 Climate Models – Part 1: Estimation of return values and their evaluation, *Nat. Hazards Earth Syst. Sci.*, 10, 907-922,
942 <https://doi.org/10.5194/nhess-10-907-2010>, 2010.

943

944 Landelius, T., Dahlgren, P., Gollvik, S., Jansson, A. and Olsson, E.: A high-resolution regional reanalysis for Europe.
945 Part 2: 2D analysis of surface temperature, precipitation and wind, *Q. J. R. Meteorol. Soc.*, 142, 2132–2142,
946 doi:10.1002/qj.2813, 2016.

947

948 Lhotka, O., Kysely, J. and Farda, A.: Climate change scenarios of heat waves in Central Europe and their uncertainties.
949 *Theor Appl Climatol.*, 131, 1043-1054, <https://doi.org/10.1007/s00704-016-2031-3>, 2018.

950

951 Matsueda, M., Mizuta, R. and Kusunoki, S.: Future change in wintertime atmospheric blocking simulated using a 20-
952 km-mesh atmospheric global circulation model, *J. Geophys. Res.*, 114, D12114, doi: 10.1029/2009JD011919, 2009.

953

954 Mizielinski, M. S., Roberts, M. J., Vidale, P. L., Schiemann, R., Demory, M.-E., Strachan, J., Edwards, T., Stephens,
955 A., Lawrence, B. N., Pritchard, M., Chiu, P., Iwi, A., Churchill, J., del Cano Novales, C., Kettleborough, J., Roseblade,
956 W., Selwood, P., Foster, M., Glover, M., and Malcolm, A.: High-resolution global climate modelling: the UPSCALE
957 project, a large-simulation campaign, *Geosci. Model Dev.*, 7, 1629–1640, doi:10.5194/gmd-7-1629-2014, 2014.

958

959 Niermann, D., Kaiser-Weiss, A., Borsche, M., van den Besselaar, E., Lussana, C., Isotta, F., Frei, C, Cantarello, L.,
960 Tveito, O. E., van der Schrier, G., Cornes, R, Vreede, E., Bojariu, R, and Davie, J.: Report for Deliverable 3.6 of the
961 UERRA project: Scientific report on assessment of regional analysis against independent data sets, pp. 138 , available
962 from: <http://www.uerra.eu/publications/deliverable-reports.html>

963

964 O'Brien, T. A., Collins, W. D., Kashinath, K., Rübel, O., Byna, S., Gu, J., Krishnan, H. and Ullrich, P. A.: Resolution
965 dependence of precipitation statistical fidelity in hindcast simulations, *J. Adv. Model. Earth Syst.*, 8, 976–990, doi:
966 10.1002/2016MS000671, 2016.

967

968 O'Reilly, C. H., Minobe, S. and Kuwano-Yoshida, A.: The influence of the Gulf Stream on wintertime European
969 blocking, *Clim. Dynam.*, 47, 1545- 1567, <https://doi.org/10.1007/s00382-015-2919-0>, 2016.

970
971 Prein, A. F. and Gobiet, A.: Impacts of uncertainties in European gridded precipitation observations on regional climate
972 analysis, *Int. J. Climatol.*, 37, 305-327, doi:10.1002/joc.4706, 2017.
973
974 Prein, A. F., Langhans, W., Fossier, G., Ferrone, A., Ban, N., Goergen, K., Keller, M., Tölle, M., Gutjahr, O., Feser,
975 F., Brisson, E., Kollet, S., Schmidli, J., Van Lipzig, N. P. M., and Leung, R.: A review on regional convection-
976 permitting climate modeling: Demonstrations, prospects, and challenges, *Rev. Geophys.*, 53, 323–361. doi:
977 10.1002/2014RG000475, 2015.
978
979 Prein, A.F., Gobiet, A., Truhetz, H., Keuler, K., Goergen, K., Teichmann, C., Fox Maule, C., van Meijgaard, E., Déqué,
980 M., Nikulin, G., Vautard, R., Colette, A., Kjellström, E., and Jacob, D.: Precipitation in the EURO-CORDEX 0.11°
981 and 0.44° simulations: high resolution, high benefits?, *Clim. Dynam.* 46, 383-412, doi: 10.1007/s00382-015-2589-y,
982 2016.
983
984 Pryor, S. C., Nikulin, G., and Jones, C.: Influence of spatial resolution on regional climate model derived wind climates,
985 *J. Geophys. Res.*, 117, D03117, doi:10.1029/2011JD016822, 2012
986
987 Risanto, C.B., Castro, C.L., Moker, J.M., Jr., Arellano, A.F., Jr., Adams, D.K., Fierro, L.M., Minjarez Sosa, C.M.:
988 Evaluating Forecast Skills of Moisture from Convective-Permitting WRF-ARW Model during 2017 North
989 American Monsoon Season. *Atmosphere*, 10, 694, doi:[10.3390/atmos10110694](https://doi.org/10.3390/atmos10110694), 2019
990
991 Roberts, M. J., Vidale, P. L., Senior, C., Hewitt, H. T., Bates, C., Berthou, S., Chang, P., Christensen, H. M., Danilov,
992 S., Demory, M. E., Griffies, S. M., Haarsma, R., Jung, T., Martin, G., Minobe, S., Ringler, T., Satoh, M., Schiemann,
993 R., Scoccimarro, E., Stephens, G. and Wehner, M.F.: The benefits of global high-resolution for climate simulation:
994 process-understanding and the enabling of stakeholder decisions at the regional scale.. *B. Am. Meteorol. Soc.*, 99,
995 2341–2359 <https://doi.org/10.1175/BAMS-D-15-00320.1>, 2018.
996
997 Ruti, P. M., Somot, S., Giorgi, F., Dubois, C., Flaounas, E., Obermann, A., Dell'Aquila, A., Pisacane, G., Harzallah,
998 A., Lombardi, E., Ahrens, B., Akhtar, N., Alias, A., Arsouze, T., Aznar, R., Bastin, S., Bartholy, J., Béranger, K.,
999 Beuvier, J., Bouffies-Cloch e, S., Brauch, J., Cabos, W., Calmanti, S., Calvet, J., Carillo, A., Conte, D., Coppola, E.,
1000 Djurdjevic, V., Drobinski, P., Elizalde-Arellano, A., Gaertner, M., Gal n, P., Gallardo, C., Gualdi, S., Goncalves, M.,
1001 Jorba, O., Jord , G., L'Heveder, B., Lebeaupin-Brossier, C., Li, L., Liguori, G., Lionello, P., Maci s, D., Nabat, P.,
1002  nol, B., Raikovic, B., Ramage, K., Sevault, F., Sannino, G., Struglia, M. V., Sanna, A., Torma, C., and Vervatis, V.:
1003 Med-CORDEX Initiative for Mediterranean Climate Studies. *B. Am. Meteorol. Soc.*, 97, 1187–1208,
1004 <https://doi.org/10.1175/BAMS-D-14-00176.1>, 2016
1005

1006 Schiemann, R., Demory, M. E., Shaffrey, L. C., Strachan, J., Vidale, P. L., Mizielinski, M. S., Roberts, M. J., Matsueda,
1007 M., Wehner, M. F. and Jung, T.: The resolution sensitivity of Northern Hemisphere blocking in four 25-km
1008 atmospheric global circulation models, *J. Climate.*, 30, 337–358, <https://doi.org/10.1175/JCLI-D-16-0100.1>, 2017.
1009

1010 Schiemann, R., Vidale, P. L., Shaffrey, L. C., Johnson, S. J., Roberts, M. J., Demory, M.-E., Mizielinski, M. S., and
1011 Strachan, J.: Mean and extreme precipitation over European river basins better simulated in a 25 km AGCM, *Hydrol.*
1012 *Earth Syst. Sci.*, 22, 3933-3950, <https://doi.org/10.5194/hess-22-3933-2018>, 2018.
1013

1014 Schiemann, R., Athanasiadis, P., Barriopedro, D., Doblas-Reyes, F., Lohmann, K., Roberts, M. J., Sein, D. V., Roberts,
1015 C. D., Terray, L., and Vidale, P. L.: Northern Hemisphere blocking simulation in current climate models: evaluating
1016 progress from the Climate Model Intercomparison Project Phase 5 to 6 and sensitivity to resolution, *Weather Clim.*
1017 *Dynam.*, 1, 277–292, <https://doi.org/10.5194/wcd-1-277-2020>, 2020.
1018

1019 Seneviratne, S. I., Nicholls, N., Easterling, D., Goodess, C. M., Kanae, S., Kossin, J., Luo, Y., Marengo, J., McInnes,
1020 K., Rahimi, M., Reichstein, M., Sorteberg, A., Vera, C. and Zhang, X.: Changes in climate extremes and their impacts
1021 on the natural physical environment. In: *Managing the Risks of Extreme Events and Disasters to Advance Climate*
1022 *Change Adaptation. A Special Report of Working Groups I and II of the Intergovernmental Panel on Climate Change*,
1023 edited by: Field, C. B., Barros, V., Stocker, T. F., Qin, D., Dokken, D. J., Ebi, K., L. Mastrandrea, M. D., Mach, K.
1024 J., Plattner, G.-K., Allen, S. K., Tignor, M. and Midgley, P. M., Cambridge University Press, Cambridge, UK, and
1025 New York, NY, USA, pp. 109-230, 2012
1026

1027 Shields, C. A., Kiehl, J. T., and Meehl, G. A.: Future changes in regional precipitation simulated by a half-degree
1028 coupled climate model: Sensitivity to horizontal resolution, *J. Adv. Model. Earth Syst.*, 8, 863–884, doi:
1029 10.1002/2015MS000584, 2016.
1030

1031 Skamarock, W.C.: Evaluating Mesoscale NWP Models Using Kinetic Energy Spectra. *Mon. Wea. Rev.*, 132, 3019–
1032 3032, <https://doi.org/10.1175/MWR2830.1>, 2004
1033

1034 Strandberg, G. and Lind, P.: The importance of model resolution on simulated precipitation in Europe – from global
1035 to regional model, *Weather Clim. Dynam. Discuss.*, <https://doi.org/10.5194/wcd-2020-31>, in review, 2020.
1036

1037 Stott, P. A., Christidis, N., Otto, F. E., Sun, Y., Vanderlinden, J., van Oldenborgh, G. J., Vautard, R., von Storch, H.,
1038 Walton, P., Yiou, P. and Zwiers, F. W.: Attribution of extreme weather and climate-related events. *WIREs Clim.*
1039 *Change*, 7, 23-41. doi:10.1002/wcc.380, 2016.
1040

1041 Strommen, K., Mavilia, I., Corti, S., Matsueda, M., Davini, P., von Hardenberg, J., Vidale, P.-L. and Mizuta, R. : The
1042 sensitivity of Euro-Atlantic regimes to model horizontal resolution. *Geophysical Research*
1043 *Letters*, 46, 7810– 7818. <https://doi.org/10.1029/2019GL082843>, 2019

1044
1045 Taylor, K., Williamson, D., and Zwiers, F.: The sea surface temperature and sea-ice concentration boundary conditions
1046 for AMIP II simulations, PCMDI Rep. 60, Tech. Rep. 60, PCMDI, 25 pp., available at: [http://www-](http://www-pcmdi.llnl.gov/publications/ab60.html)
1047 [pcmdi.llnl.gov/publications/ab60.html](http://www-pcmdi.llnl.gov/publications/ab60.html), 2000.
1048
1049 Taylor, K. E., Stouffer, R. J. and Meehl, G. A.: An overview of CMIP5 and the experiment design, *B. Am. Meteorol.*
1050 *Soc.*, 93, 485498, doi: 10.1175/BAMS-D-11-00094.1, 2012.
1051
1052 Terai, C. R., Caldwell, P. M., Klein, S. A. Tang, Q. and Branstetter, M. L.: The atmospheric hydrologic cycle in the
1053 ACME v0.3 model. *Clim. Dynam.*, 50, 3251- 3279. <https://doi.org/10.1007/s00382-017-3803-x>, 2018.
1054
1055 Torma, C., Giorgi, F. and Coppola, E.: Added value of regional climate modeling over areas characterized by complex
1056 terrain—Precipitation over the Alps, *J. Geophys. Res. Atmos.*, 120, 3957–3972, doi: 10.1002/2014JD022781, 2015.
1057
1058 van der Linden, E. C., Haarsma, R. J., and van der Schrier, G.: Impact of climate model resolution on soil moisture
1059 projections in central-western Europe, *Hydrol. Earth Syst. Sci.*, 23, 191–206, [https://doi.org/10.5194/hess-23-191-](https://doi.org/10.5194/hess-23-191-2019)
1060 2019, 2019.
1061
1062 Van Haren, R., Haarsma, R. J., Van Oldenborgh, G. J. and Hazeleger, W.: Resolution Dependence of European
1063 Precipitation in a State-of-the-Art Atmospheric General Circulation Model, *J. Climate.*, 28, 5134–5149, doi:
1064 10.1175/JCLI-D-14-00279.1, 2015a.
1065
1066 Van Haren, R., Haarsma, R. J., de Vries, H., van Oldenborgh, G. J., and Hazeleger, W.: Resolution dependence of
1067 circulation forced future central European summer drying, *Environ. Res. Lett.*, 10, 055002, doi:10.1088/1748-
1068 9326/10/5/055002, 2015b.
1069
1070 Vanniere, B., Vidale, P. L., Demory, M.-E., Schiemann, R., Roberts, M. J., Roberts, C. D., Matsueda, M., Terray, L.,
1071 Koenigk, T., Senan, R.: Multi-model evaluation of the sensitivity of the global energy budget and hydrological cycle
1072 to resolution, *Clim. Dynam.*, 52, 6817- 6846, <https://doi.org/10.1007/s00382-018-4547-y>, 2019
1073
1074 Vautard, R., Gobiet, A., Jacob, D., Belda, M., Colette, A., Déqué, M., Fernández, J., García-Díez, M., Goergen, K.,
1075 Güttler, I., Halenka, T., Karacostas, T., Katragkou, E., Keuler, K., Kotlarski, S., Mayer, S., van Meijgaard, E., Nikulin,
1076 G., Patarcic, M., Scinocca, J., Sobolowski, S., Suklitsch, M., Teichmann, C., Warrach-Sagi, K., Wulfmeyer, V., Yiou,
1077 P. : The simulation of European heat waves from an ensemble of regional climate models within the EURO-CORDEX
1078 project, *Clim. Dynam.*, 41, 2555-2575, doi: 10.1007/s00382-013-1714-z, 2013.
1079

1080 Vautard, R., Yiou, P., Otto, F., Stott, P., Christidis, N., van Oldenborgh, G. J. and Schaller, N.: Attribution of human-
1081 induced dynamical and thermodynamical contributions in extreme weather events, *Environ. Res. Lett.*, 11, 114009,
1082 <https://doi.org/10.1088/1748-9326/11/11/114009>, 2016.
1083

1084 Volosciuk, C., Maraun, D., Semenov, V.A. and Park, W.: Extreme Precipitation in an Atmosphere General Circulation
1085 Model: Impact of Horizontal and Vertical Model Resolutions, *J. Climate.*, 28, 1184–1205,
1086 <https://doi.org/10.1175/JCLI-D-14-00337.1>, 2015.
1087

1088 Vries, H. de, Scher, S., Haarsma, R., Drijfhout, S., and Delden, A. van.: How Gulf-Stream SST-fronts influence
1089 Atlantic winter storms, *Clim. Dynam.*, 52, 5899-5909. <https://doi.org/10.1007/s00382-018-4486-7>, 2019
1090

1091 Wehner, M. F., Smith, R. L., Bala, G. and Duffy, P.: The effect of horizontal resolution on simulation of very extreme
1092 US precipitation events in a global atmosphere model, *Clim. Dynam.*, 34, 241-247. [https://doi.org/10.1007/s00382-](https://doi.org/10.1007/s00382-009-0656-y)
1093 [009-0656-y](https://doi.org/10.1007/s00382-009-0656-y), 2010.
1094

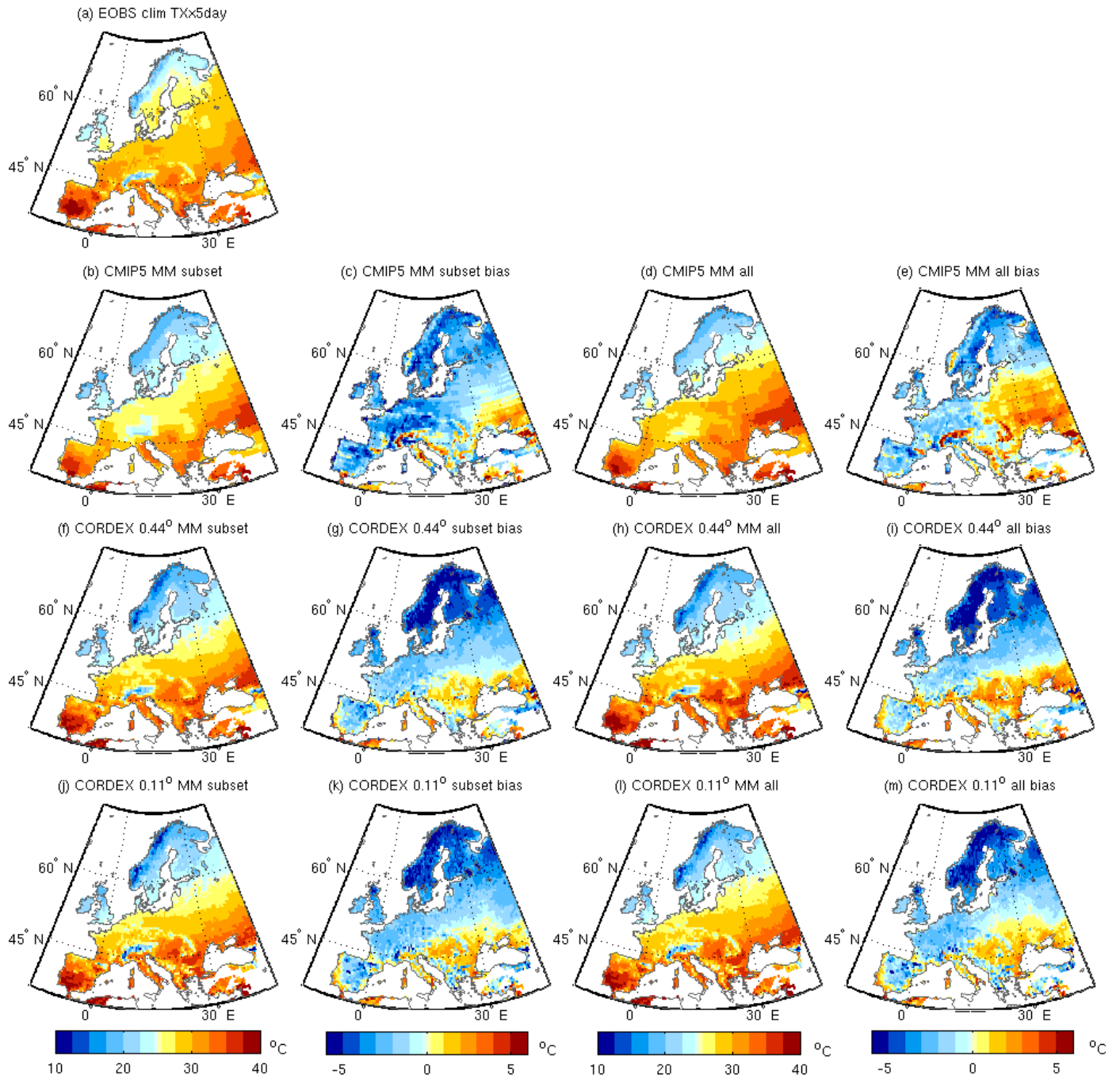
1095 Wehner, M. F., Reed, K. A., Li, F., Prabhat, Bacmeister, J., Chen, C.-T., Paciorek, C., Gleckler, P. J., Sperber, K. R.,
1096 Collins, W. D., Gettelman, A., and Jablonowski, C.: The effect of horizontal resolution on simulation quality in the
1097 Community Atmospheric Model, CAM5.1, *J. Adv. Model. Earth Syst.*, 6, 980–997, doi:10.1002/2013MS000276,
1098 2014.
1099

1100 Willison, J., Robinson, W.A. and Lackmann, G.M.: North Atlantic Storm-Track Sensitivity to Warming Increases with
1101 Model Resolution., *J. Climate.*, 28, 4513–4524, <https://doi.org/10.1175/JCLI-D-14-00715.1>, 2015.
1102

1103 Zappa, G., Shaffrey, L. C. and Hodges, K. I., The Ability of CMIP5 Models to Simulate North Atlantic Extratropical
1104 Cyclones, *J. Climate.*, 26, 5379-5396, doi: 10.1175/JCLI-D-12-00501.1, 2013.
1105

1106 Zhang, X., Alexander, L., Hegerl, G. C., Jones, P., Tank, A. K., Peterson, T. C. Trewin, B. and Zwiers, F. W.: Indices
1107 for monitoring changes in extremes based on daily temperature and precipitation data, *Wiley Interdiscip. Rev., Clim.*
1108 *Chang.*, 2, 851–870, doi:10.1002/wcc.147, 2011.
1109

1110 **Figures**



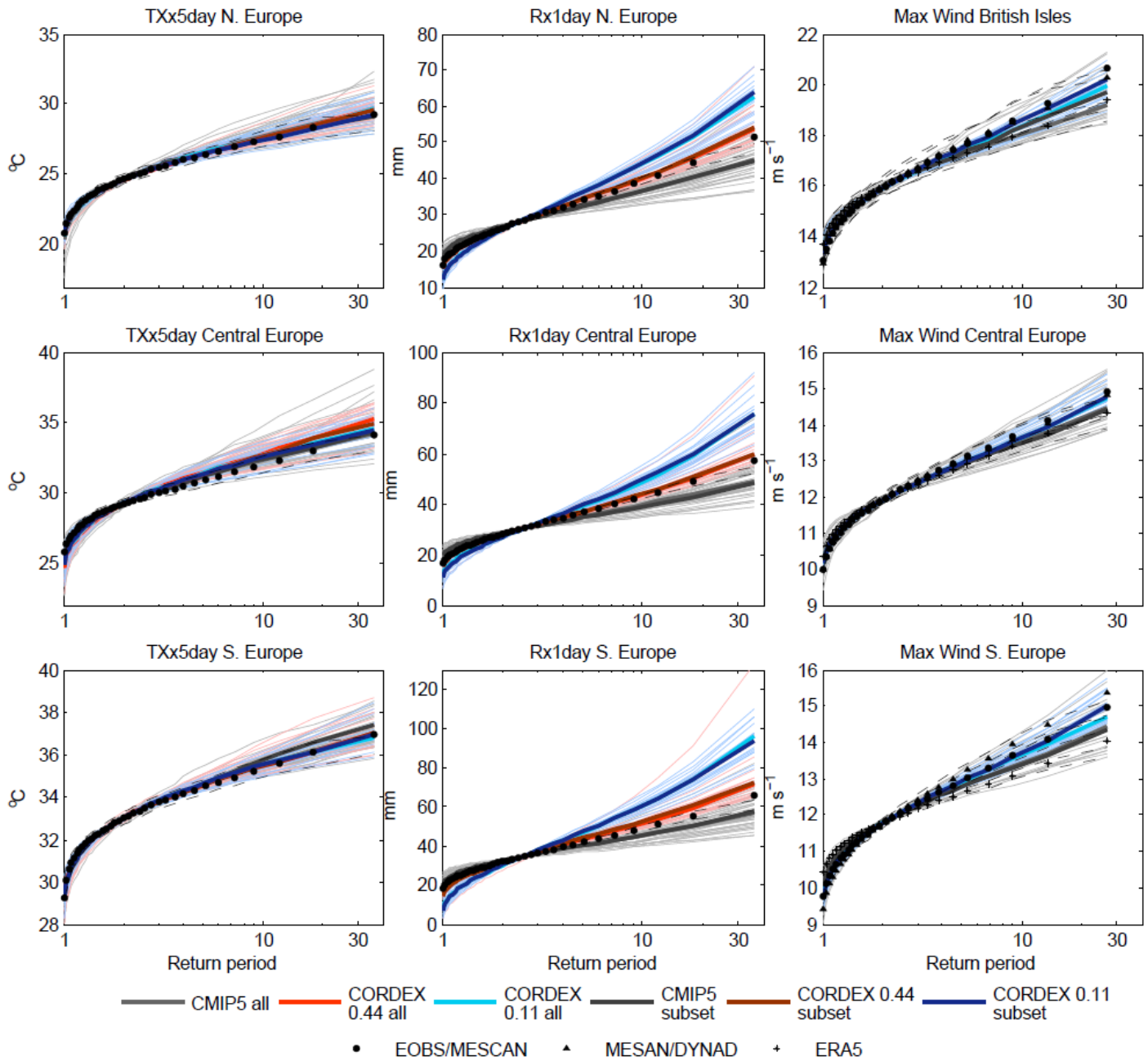
1111

1112 **Figure 1: Climatological mean of TXx5day for the period 1970-2005 for (a) E-OBS; the multi model median of the common**

1113 **subset of models (see Methods) for (b) CMIP5, (f) CORDEX 0.44° and (j) CORDEX 0.11°, (c, g, k) their biases with respect**

1114 **to E-OBS, and (d,e,h,i,j,k) the same for the full ensembles of CMIP5 and CORDEX. Units °C.**

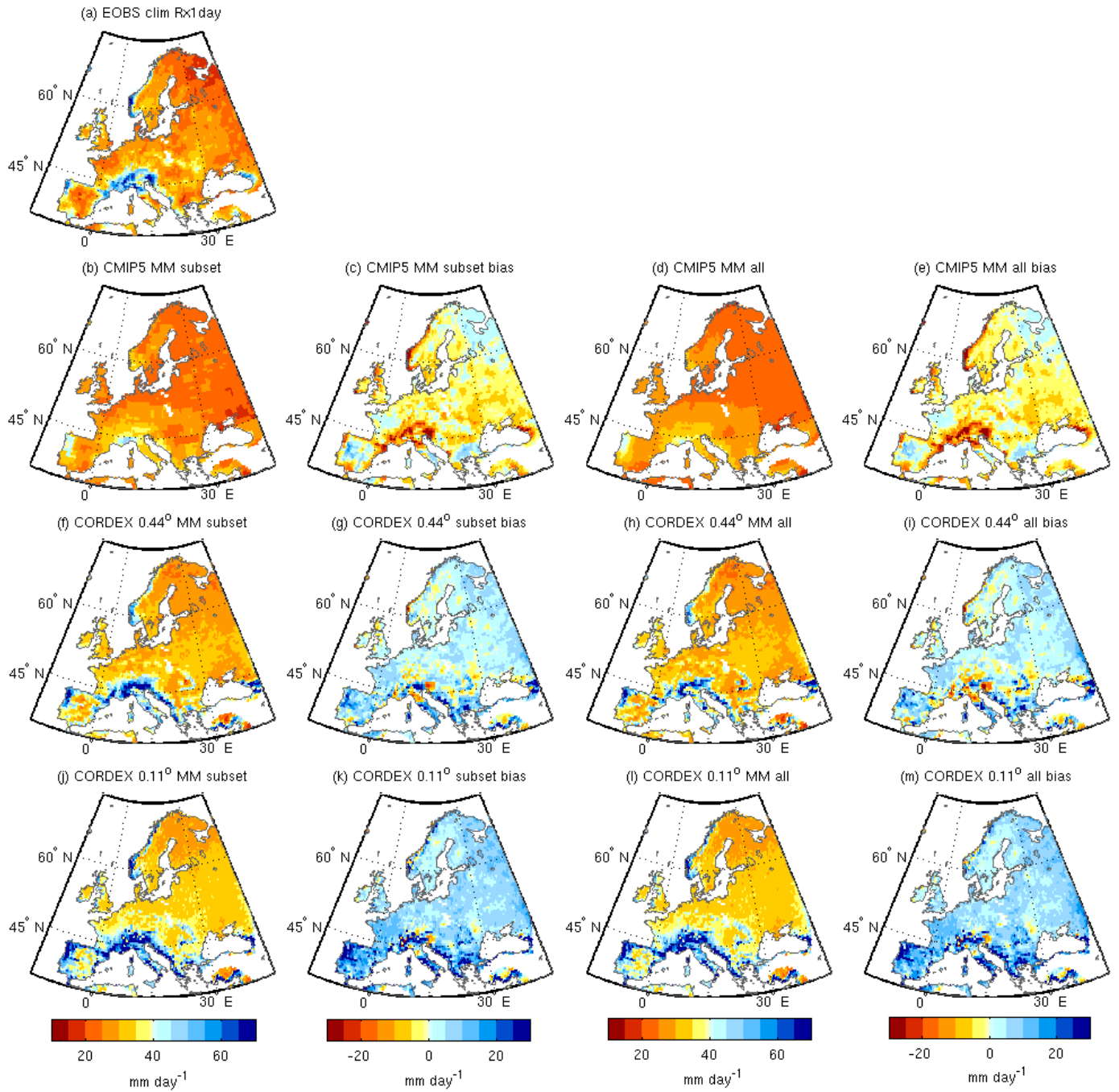
1115



1116

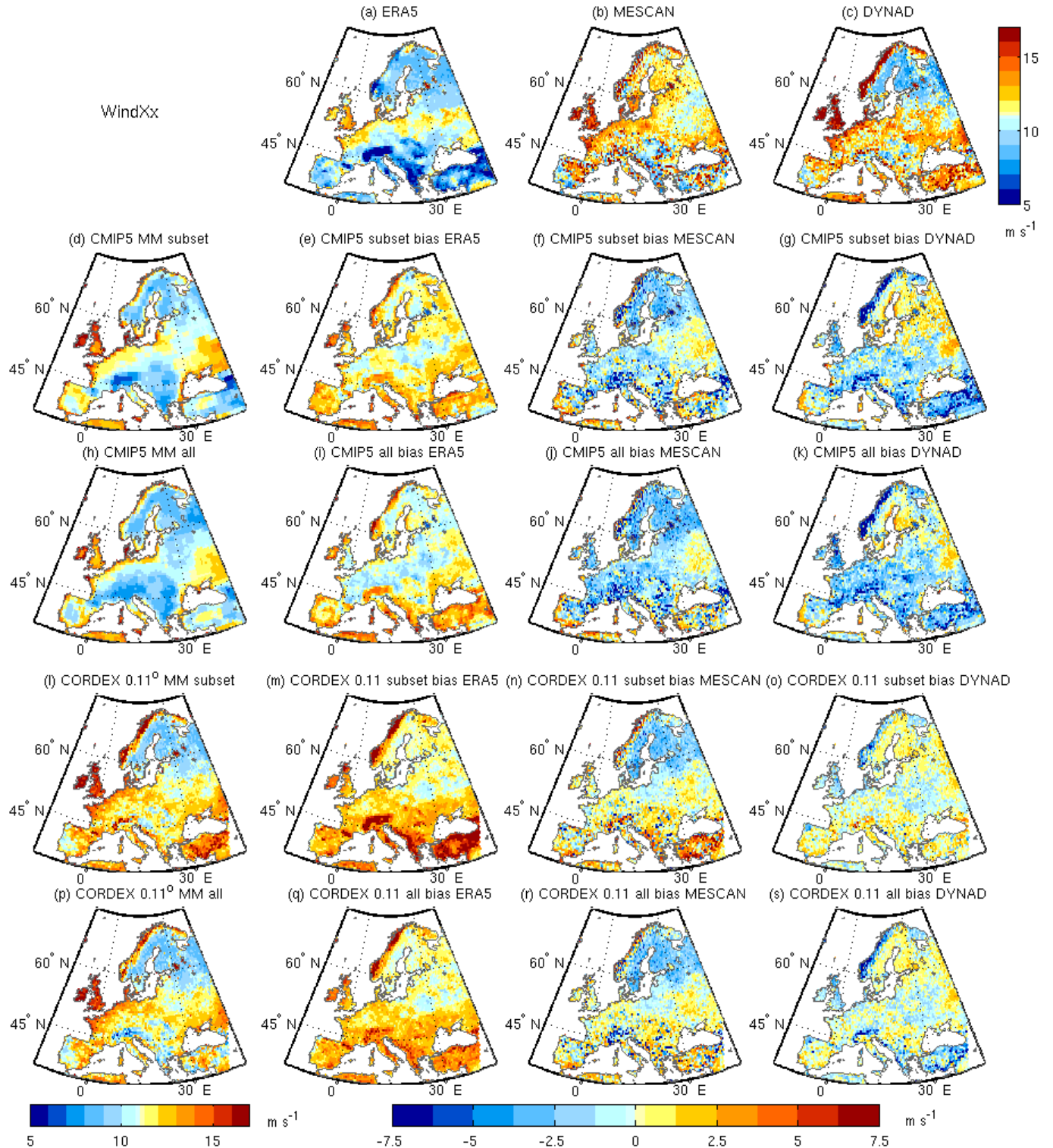
1117 **Figure 2: Return period plots for (left) TXx5day, (middle column) Rx1day and (right) annual maximum wind, for CMIP5**
 1118 **and CORDEX for Northern Europe (top row (except top right = British Isles)), Central Europe (middle row) and Southern**
 1119 **Europe (bottom row). CMIP5 is shown in grey, CORDEX 0.44° in red and CORDEX 0.11° in blue. Thin lines are individual**
 1120 **ensemble members, thick lines are multi model medians: lighter colours for the full ensembles, and darker colours for the**
 1121 **subset of models common to CMIP5 and both CORDEX resolutions. Observational datasets are shown in black, circles for**
 1122 **E-OBS temperature and precipitation and MESCAN wind, triangles for MESAN precipitation and DYNAD wind and**
 1123 **crosses for ERA5 wind. Confidence intervals based on bootstrapping are shown with dashed lines for the observational**
 1124 **datasets. The time periods considered are 1970-2005 for TXx5day and Rx1day, and 1979-2005 for wind.**

1125

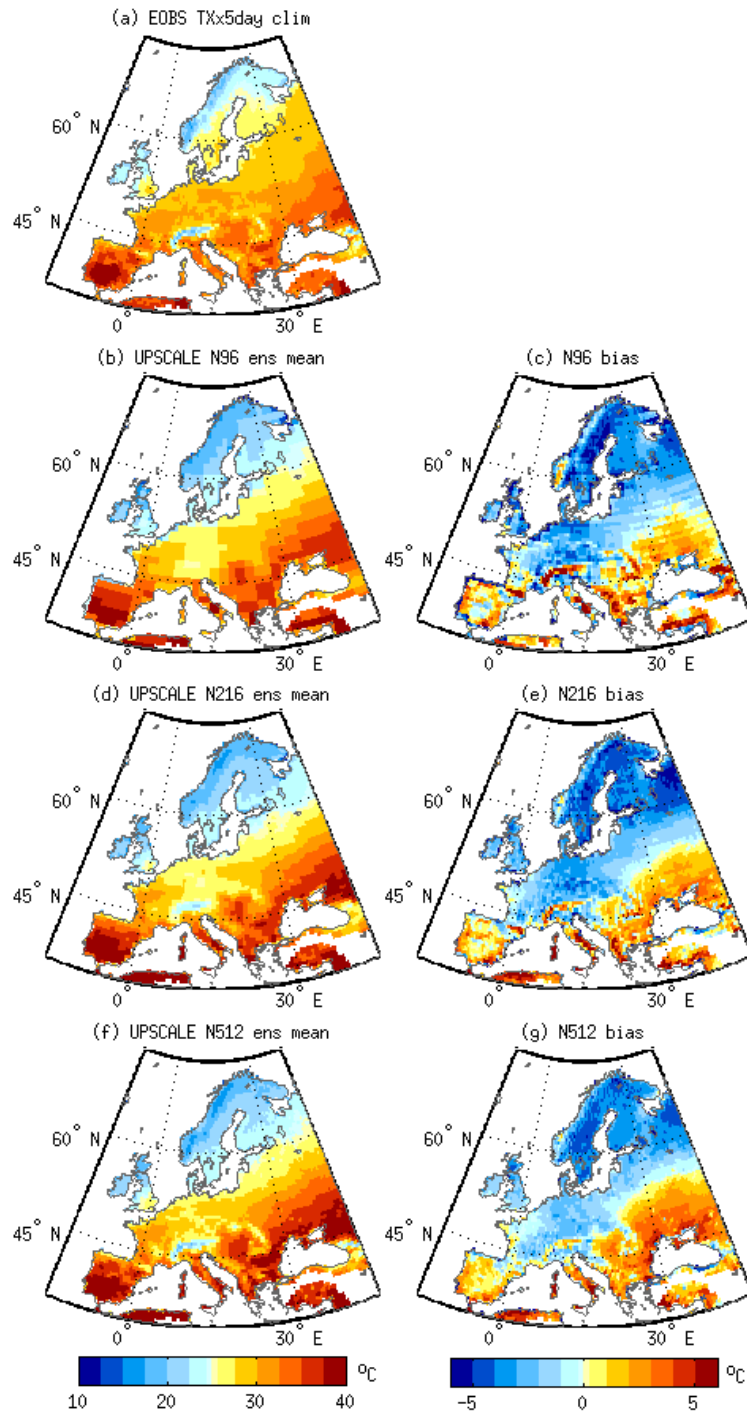


1126

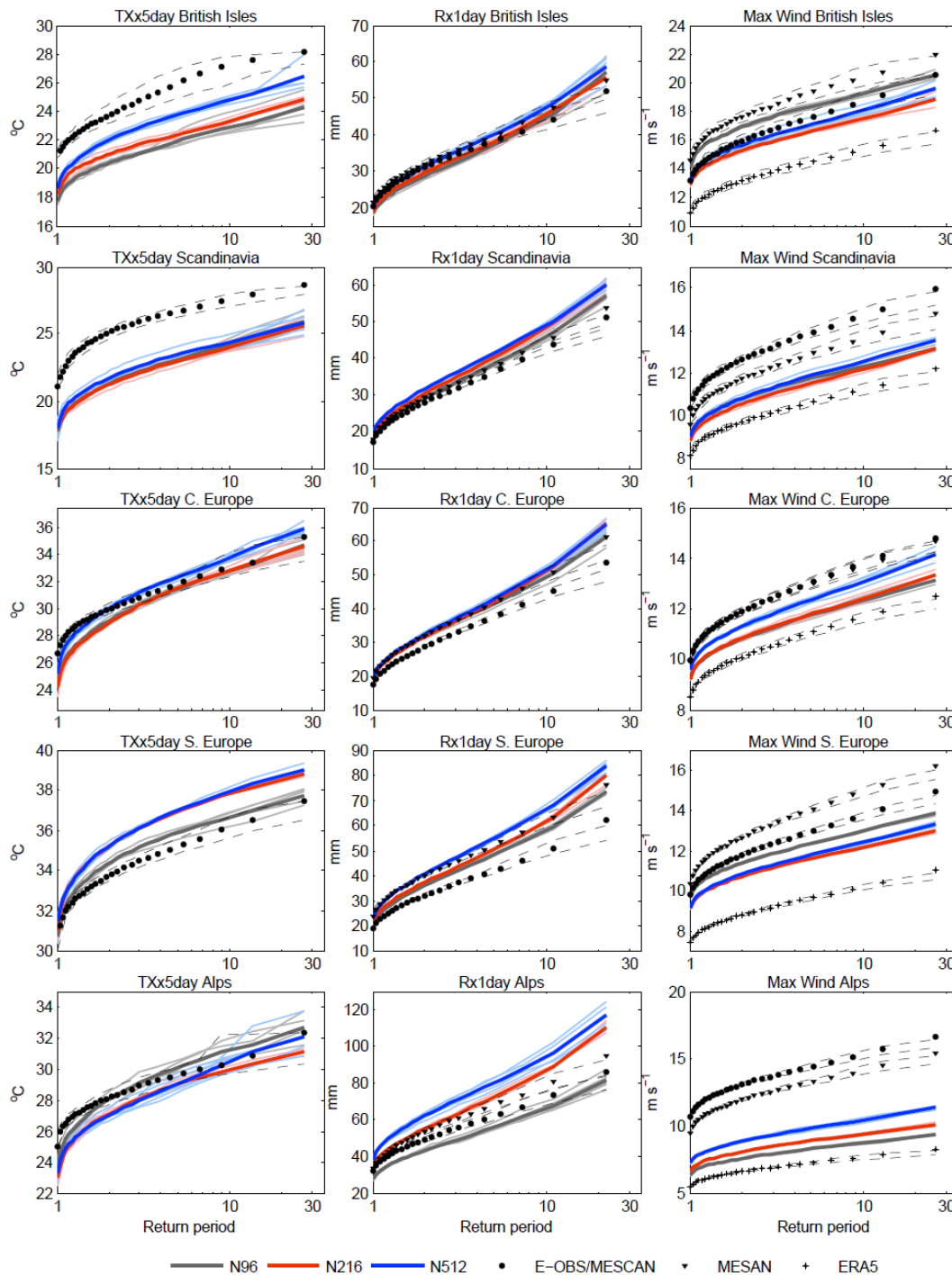
1127 **Figure 3: As for Figure 1 but for the climatological mean of Rx1day. Units mm.**



1128
 1129 **Figure 4: Climatological mean of annual maximum wind for the period 1979-2005 for (a) ERA5, (b) MESCAN (c)**
 1130 **DYNAD, and for the multi model median of the common subset of models for (d) CMIP5 and (l) CORDEX 0.11° and their**
 1131 **biases with respect to the reanalyses datasets (e-g and m-o). (h-k and p-s) are the same but for the full ensembles of**
 1132 **CMIP5 and CORDEX. Units meters per second.**



1135 **Figure 5:** Climatological mean of Txx5day for the ensemble means of three resolutions of HadGEM3-A (UPSCALE) GCM simulations (left) for the period 1985-2011 and their biases with respect to E-OBS (right). (a) E-OBS, (b, c) N96 (130 km), (d, e) N216 (60 km), (f, g) N512 (25 km). Units °C.

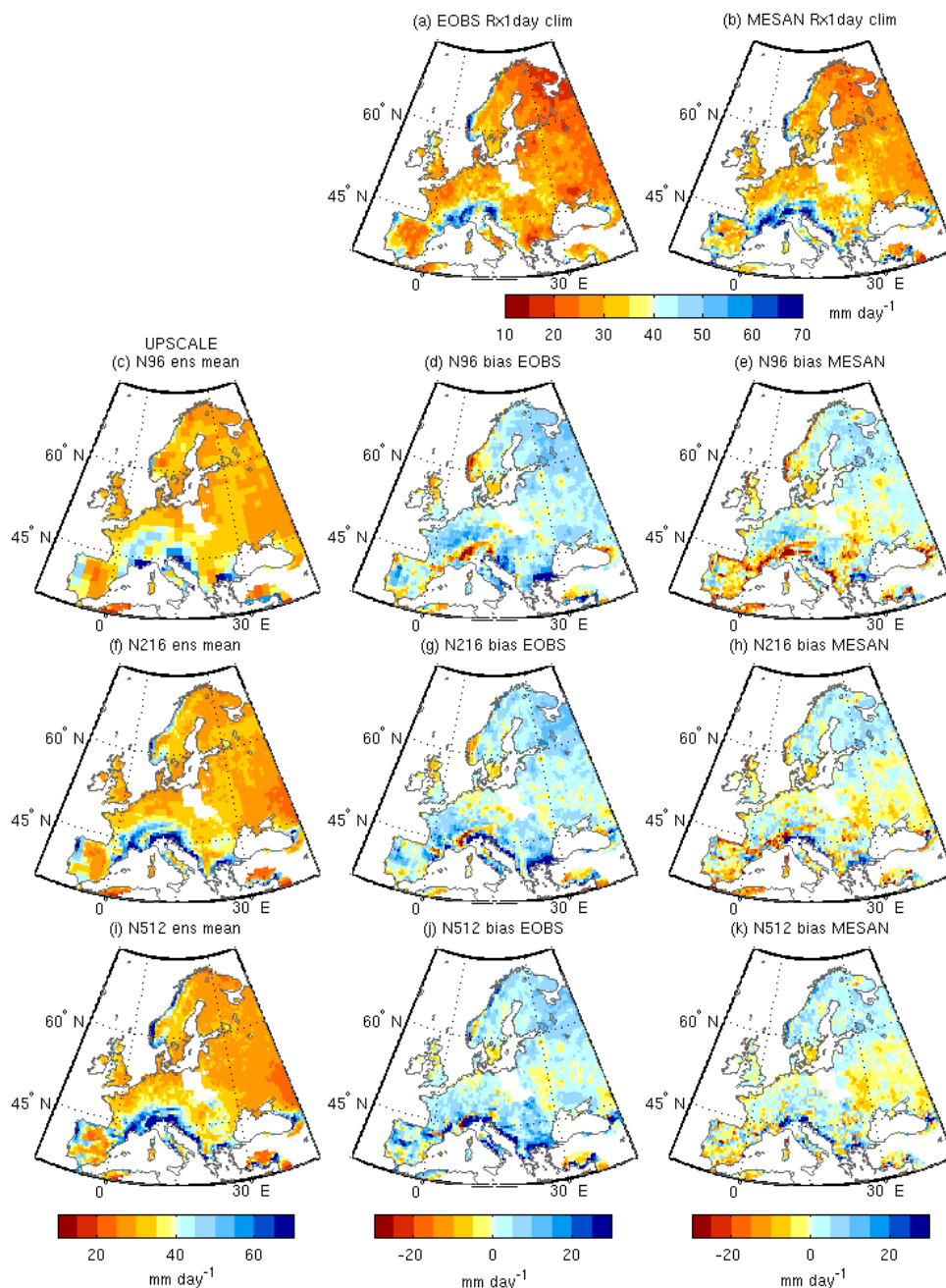


— N96 — N216 — N512 • E-OBS/MESCAN ▼ MESAN + ERA5

Figure 6: Return period plots for (left) TXx5day, middle column Rx1day and (right) annual maximum wind, for the UPSCALE simulations for (top row) the British Isles, (2nd row) Scandinavia, (3rd row) Central Europe, (4th row) Southern Europe, and (last row) the Alps. N96 is shown in grey, N216 in red and N512 in blue. Thin lines are individual ensemble members, thick lines represent

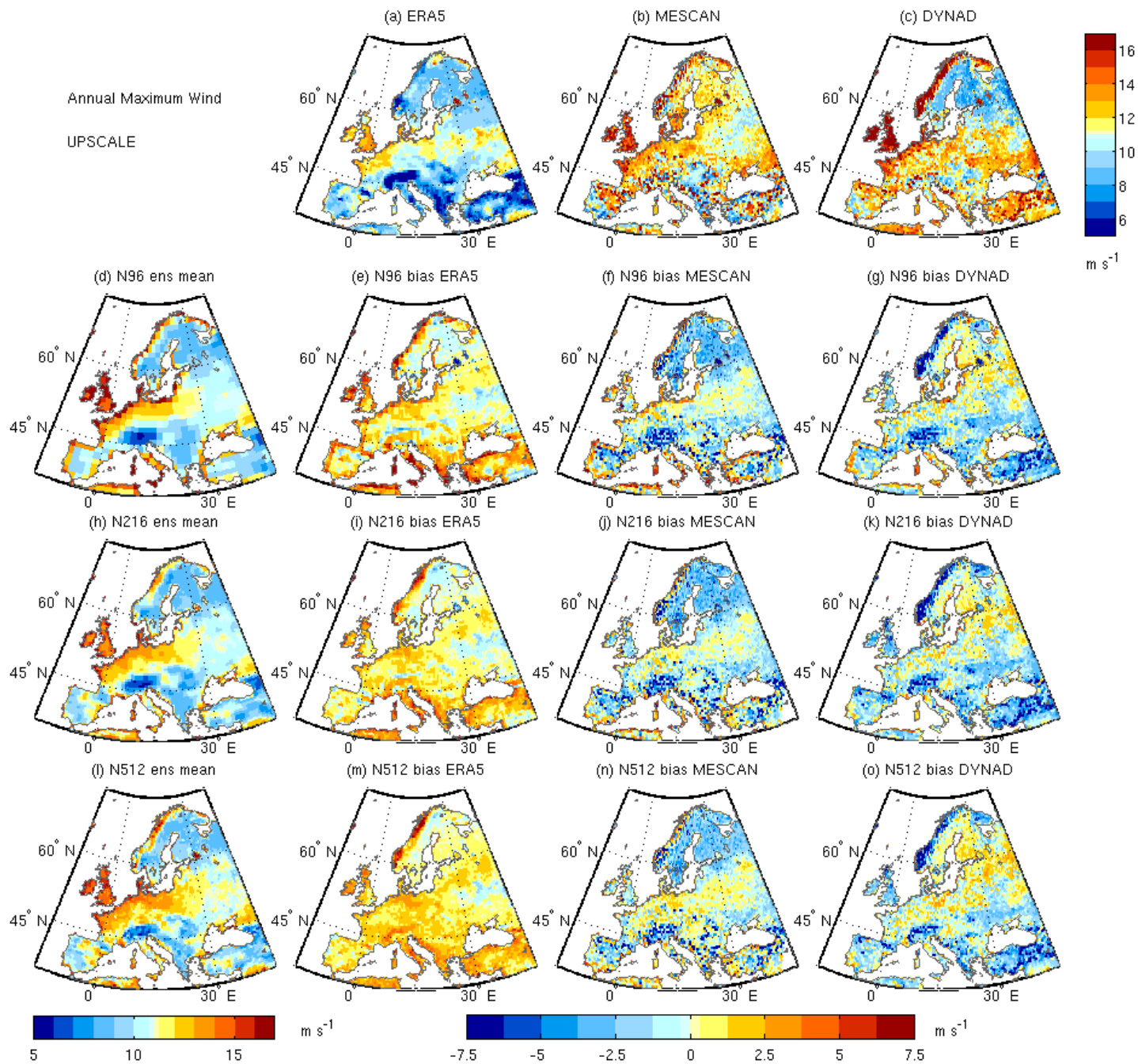
1140

ensemble means. Observational datasets are shown in black, circles for E-OBS and MESCAN, triangles for MESAN and DYNAD, and asterisks for ERA5. Confidence intervals based on bootstrapping are shown with dashed lines for the observational datasets. The time periods considered are 1985-2011 for TXx5day, 1989-2010 for Rx1day, and 1986-2011 for wind. NB: in contrast to Figure 2 the curves have not been shifted to have the same mean value (see methods), see Figure S10 for the shifted version.



1145

Figure 7: Climatological mean of Rx1day for the ensemble means of three resolutions of UPSCALE (left) simulations for the period 1989-2010 and their biases with respect to E-OBS (middle) and the MESAN reanalysis (right). (a) E-OBS, (b) MESAN (c-e) N96, (f-h) N216, (i-k) N512. Units mm.



1150 **Figure 8: Climatological mean of annual maximum wind for the ensemble means of three resolutions of UPSCALE (left) simulations for the period 1986-2011 and their biases with respect to the observational datasets ERA5 (left column), MESCAN (middle) and MESAN (right). (a) ERA5, (b) MESCAN (c) DYNAD, (d-g) N96, (h-k) N216, (l-o) N512. Units meters per second.**

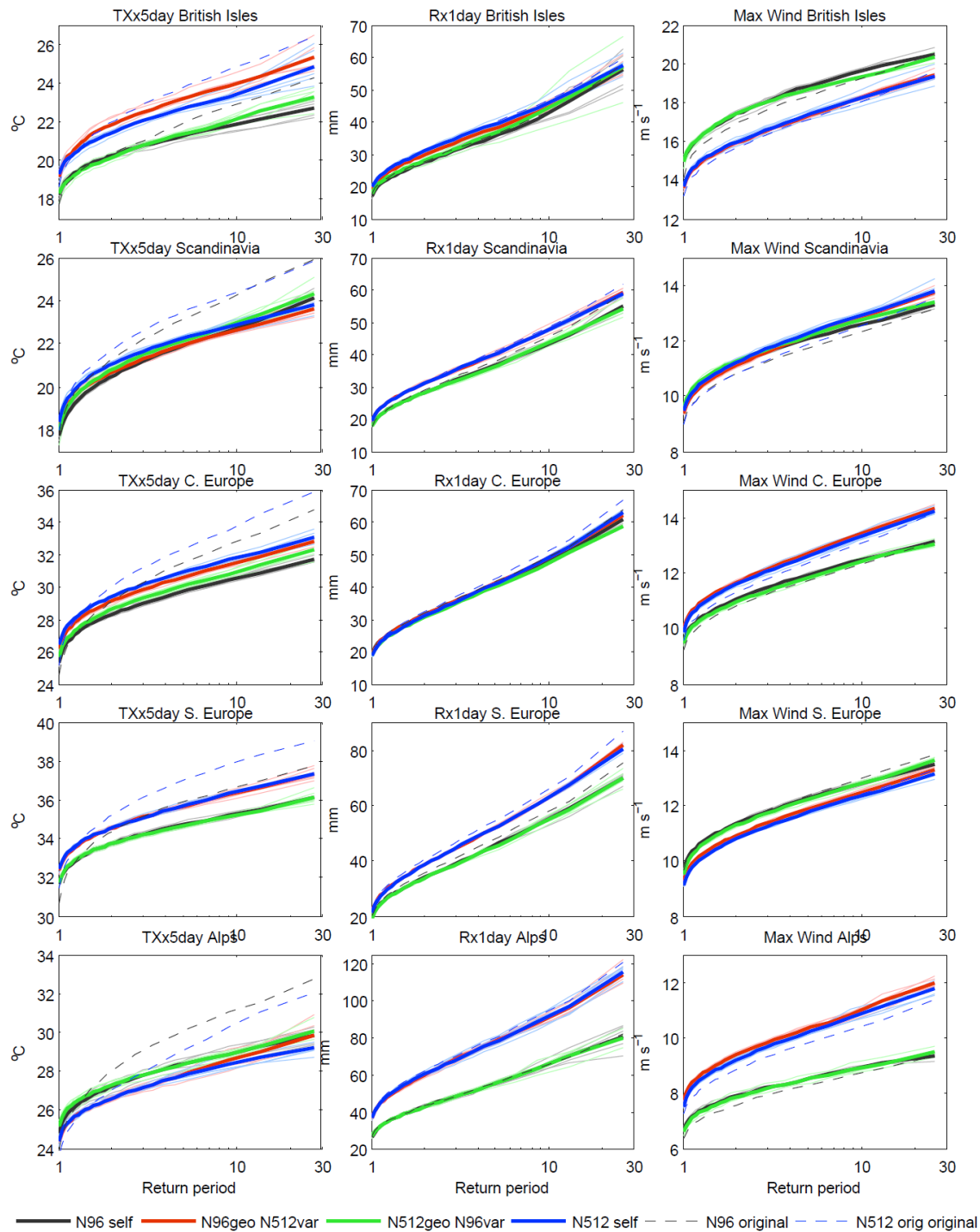


Figure 9: Circulation analogue results. Return period plots for (left) TXx5day, (middle) Rx1day and (right) annual maximum wind for (top) the British Isles, (2nd row) Scandinavia, (3rd row) Central Europe, (4th row) Southern Europe and (5th row) the Alps. Grey represents the N96 self-analogues, blue the N512 self-analogues, red is for N96 circulation with N512 variables (e.g. precipitation)

and green is for N512 circulation with N96 variables. Thin lines represent individual ensemble members, thick lines represent the mean across individual ensemble members. Blue dashed line represents the original N512 ensemble mean results like those shown in Figure 6 (although sometimes based on a different time period), and the grey dashed lines represent the equivalent for the N96 simulations. Results for TXx5day are based on the period 1985-2011, Rx1day 1986-2011, and wind 1986-2011.

1160